



DIFFUSER STUDIES

Delbert Taylor, David A. Duesterhaus, and Marvin Simmons
ARO, Inc.

ENGINE TEST FACILITY
ARNOLD ENGINEERING DEVELOPMENT CENTER
AIR FORCE SYSTEMS COMMAND
ARNOLD AIR FORCE STATION, TENNESSEE 37389

February 1974

Final Report for Period July 1, 1972 – June 30, 1973

Approved for public release; distribution unlimited.

Property of U. S. Air Force
AEDC LIBRARY
F40600-74-C-0001

Prepared for

ARNOLD ENGINEERING DEVELOPMENT CENTER (XON)
ARNOLD AIR FORCE STATION, TENNESSEE 37389

NOTICES

When U. S. Government drawings specifications, or other data are used for any purpose other than a definitely related Government procurement operation, the Government thereby incurs no responsibility nor any obligation whatsoever, and the fact that the Government may have formulated, furnished, or in any way supplied the said drawings, specifications, or other data, is not to be regarded by implication or otherwise, or in any manner licensing the holder or any other person or corporation, or conveying any rights or permission to manufacture, use, or sell any patented invention that may in any way be related thereto.

Qualified users may obtain copies of this report from the Defense Documentation Center.

References to named commercial products in this report are not to be considered in any sense as an endorsement of the product by the United States Air Force or the Government.

APPROVAL STATEMENT

This technical report has been reviewed and is approved.


ELTON R. THOMPSON
Research and Development
Division
Directorate of Technology


ROBERT O. DIETZ
Director of Technology

UNCLASSIFIED

SECURITY CLASSIFICATION OF THIS PAGE(When Data Entered)

section of the variable-geometry ejector was also evaluated, and its performance was compared with that of the variable-area ejectors. The optimum performance of all variable-area ejectors exceeded that of the cylindrical ejector. The pressure recovery of a sonic airflow meter having a subsonic exit diffuser efflux angle of 10 deg was evaluated with diffuser exit-to-inlet area ratios of 3.16 and 4.10, both with and without exit tailpipes. The effect of tailpipes on pressure loss was insignificant.

AFSC
Annex AFS Term

UNCLASSIFIED

SECURITY CLASSIFICATION OF THIS PAGE(When Data Entered)

PREFACE

The work reported herein was conducted by the Arnold Engineering Development Center (AEDC), Air Force Systems Command (AFSC). The results were obtained by ARO, Inc. (a subsidiary of Sverdrup & Parcel and Associates, Inc.), contract operator of AEDC, AFSC, Arnold Air Force Station, Tennessee. The work was done under ARO Project No. RF226. The manuscript (ARO Control No. ARO-ETF-TR-73-139) was submitted for publication on October 19, 1973.

CONTENTS

	<u>Page</u>
1.0 INTRODUCTION	7
2.0 APPARATUS	8
3.0 PROCEDURE	23
4.0 RESULTS AND DISCUSSION	24
5.0 SUMMARY OF RESULTS	39
REFERENCES	40

ILLUSTRATIONS

Figure

1. Typical Installation of Test Hardware	8
2. Primary Nozzle Details	9
3. Details of Constant-Area Ejector	10
4. Variable-Area Ejector with Double-Angle Centerbody	11
5. Double-Angle Centerbody	
a. Details	12
b. Flow Area versus Axial Position	12
c. Second-Throat Area versus Centerbody Position	13
6. Variable-Area Ejector with Triple-Angle Centerbody	13
7. Triple-Angle Centerbody	
a. Details	14
b. Flow Area versus Axial Position	14
c. Second-Throat Area versus Centerbody Position.	15
8. Variable-Area Ejector with Single-Angle Centerbody	16
9. Single-Angle Centerbody	
a. Details	16
b. Flow Area versus Axial Position.	17
c. Second-Throat Area versus Centerbody Position.	17

<u>Figure</u>	<u>Page</u>
10. Test Section with Typical Venturi Installation	18
11. Venturi Inlet Total Pressure Probe Arrangement	18
12. Venturi Exit Total Pressure Probe Arrangement	19
13. Details of Air-Metering Venturis	
a. $A_{ve}/A^* = 4.10$	20
b. $A_{ve}/A^* = 3.16$	20
14. Details of Diffuser Tailpipe	
a. $A_{ve}/A^* = 4.10$	21
b. $A_{ve}/A^* = 3.16$	21
15. Typical Venturi Installation with Tailpipe	22
16. Ejector Exit Total Pressure Probe Arrangement	23
17. Typical Ejector Characteristics	25
18. Constant-Area Ejector Characteristic	
a. $A_d/A^* = 3.987$	26
b. $A_d/A^* = 5.756$	26
19. Double-Angle Centerbody Variable-Area Ejector Starting Characteristics	27
20. Double-Angle Centerbody Variable-Area Ejector Axial Static Pressure, $\dot{m}''/\dot{m}' = 10$ percent, $A_d/A^* = 3.987$	27
21. Triple-Angle Centerbody Variable-Area Ejector, $A_d/A^* = 3.987$	
a. Overall Performance	28
b. Performance Compared with Constant-Area Ejector, $\dot{m}''/\dot{m}' = 0$ percent	28
c. Performance Compared with Constant-Area Ejector, $\dot{m}''/\dot{m}' = 5$ percent	28
d. Performance Compared with Constant-Area Ejector, $\dot{m}''/\dot{m}' = 10$ percent	28
22. Triple-Angle Centerbody Variable-Area Ejector, $A_d/A^* = 5.756$	
a. Overall Performance	29
b. Performance Compared with Constant-Area Ejector, $\dot{m}''/\dot{m}' = 0$ percent	29

<u>Figure</u>	<u>Page</u>
22. Continued	
c. Performance Compared with Constant-Area Ejector, $\dot{m}''/\dot{m}' = 5$ percent	29
d. Performance Compared with Constant-Area Ejector, $\dot{m}''/\dot{m}' = 10$ percent.	29
23. Triple-Angle Centerbody Variable-Area Ejector Axial Static Pressure, $\dot{m}''/\dot{m}' = 10$ percent, $A_d/A^* = 3.987$	30
24. Single-Angle Centerbody Variable-Area Ejector, $A_d/A^* = 3.987$	
a. Overall Performance	31
b. Performance Compared with Constant-Area Ejector, $\dot{m}''/\dot{m}' = 0$ percent	31
c. Performance Compared with Constant-Area Ejector, $\dot{m}''/\dot{m}' = 5$ percent	31
d. Performance Compared with Constant-Area Ejector, $\dot{m}''/\dot{m}' = 10$ percent.	31
25. Single-Angle Centerbody Variable-Area Ejector, $A_d/A^* = 5.756$	
a. Overall Performance	32
b. Performance Compared with Constant-Area Ejector, $\dot{m}''/\dot{m}' = 0$ percent	32
c. Performance Compared with Constant-Area Ejector, $\dot{m}''/\dot{m}' = 5$ percent	32
d. Performance Compared with Constant-Area Ejector, $\dot{m}''/\dot{m}' = 10$ percent.	32
26. Single-Angle Centerbody Variable-Area Ejector Axial Static Pressure, $\dot{m}''/\dot{m}' = 10$ percent, $A_d/A^* = 3.987$	33
27. Single-Angle Centerbody Configuration Performance, $A_d/A^* = 5.756$, $\dot{m}''/\dot{m}' = 5$ percent	35
28. Venturi Performance	
a. $A_{ve}/A^* = 4.10$	36
b. $A_{ve}/A^* = 3.16$	37
29. Typical Static Pressure Survey	37
30. Typical Venturi Inlet Total Pressure Profile	38
31. Typical Venturi Exit Total Pressure Profile	38
NOMENCLATURE	41

1.0 INTRODUCTION

The thrust level of aircraft gas turbine engines is increasing steadily, and as a result, ground test facilities used to develop and/or proof-test these engines at simulated flight conditions are rapidly becoming obsolete. The cost of modifying existing facilities or providing new ones is very high. Therefore, a continuing effort is made at AEDC to develop and employ methods to effect the maximum facility operating efficiency in order to extend and maximize its performance capability at minimum cost.

The number of first-stage exhaust compressors, the overall exhaust system pressure ratio, and the power required to accomplish a given test requirement are functions of many variables including system pressure losses. Therefore, in direct-connect turbojet testing, engine exhaust gas ejector-diffusers, such as those used at the AEDC, use the kinetic energy in the engine exhaust jet to pump cooling air from the test cell and efficiently convert the kinetic energy in the mixture of engine exhaust gas and cooling air to pressure at the inlet to the test facility exhaust system. The use of a single, fixed-geometry ejector over the entire power range of an augmented (afterburning) engine is undesirable because of the variation in the sonic flow area of the engine nozzle which, during maximum power, is approximately 1.5 times that corresponding to military (nonafterburning) power; therefore, the optimum ejector should have equal or larger variability to provide control of simulated altitude pressure and adequate test cell cooling flow.

Another difficulty experienced with a fixed-geometry ejector occurs during engine power transients and is directly related to the time constant of the plant exhaust system, which is large as a result of the large distributed volume between test cell and exhaust compressors. The use of a fixed-geometry ejector complicates the plant control function during engine power transients because the transients occur within one-third to one-half the time required for the plant exhaust system pressure to change. As a result, the ejector evacuates the test cell, thus causing an uncontrolled change in the simulated altitude pressure during the engine power transient. These problems can be resolved by the application of a properly configured variable second-throat ejector-diffuser.

Venturis operating at sonic conditions are employed in the plant air supply system to effect accurate measurement over a large range of airflow. These venturis employ subsonic diffusers to minimize the

metering system pressure loss; however, the diffuser expansion ratio (exit area/inlet area) required to facilitate the installation of a large number of venturis in the air supply duct is small, and since diffuser pressure loss varies inversely with expansion ratio, the venturi pressure loss may exceed the optimum attainable. The literature indicates that the pressure loss in subsonic diffusers may be minimized by the addition of tailpipes; therefore, an experimental evaluation of the pressure loss in venturis with and without tailpipes is highly desirable.

This report presents the results of an experimental evaluation of a constant-area ejector-diffuser and three configurations of a variable-area ejector-diffuser at secondary-to-primary mass flow ratios of 0, 5, 10, and 15 percent.

An experimental evaluation of a venturi equipped with and without tailpipes having area expansion ratios of 3.16 and 4.10 is also presented.

2.0 APPARATUS

2.1 INSTALLATION

The overall test hardware installation with the double-angle centerbody ejector installed to depict diffuser location is shown in Fig. 1. The test cell was fabricated from nominal 20-in.-diam pipe, 20 in. in length with standard pipe flanges. The upstream end of the test cell was sealed by a flange that supported the 10-in.-diam primary airflow duct. The seal at the downstream end was provided by the mounting flange of the ejector section.

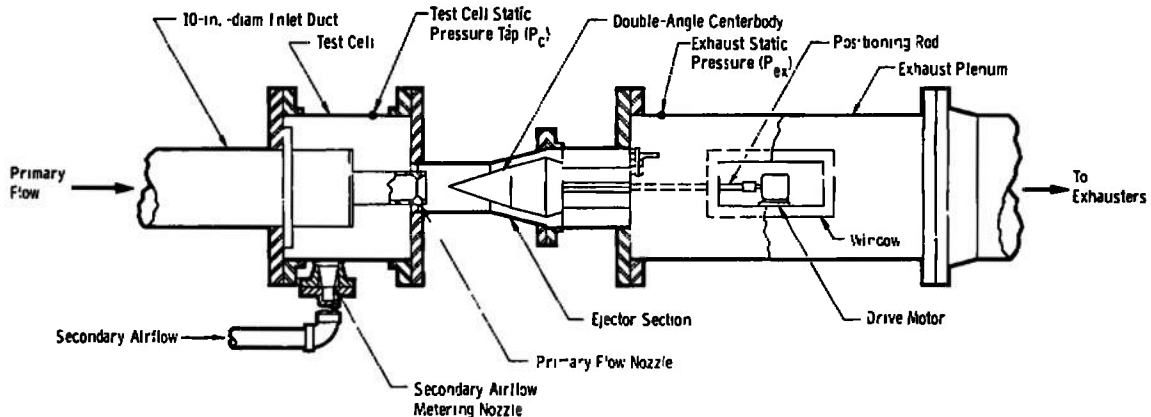


Figure 1. Typical installation of test hardware.

Coupled to the downstream end of the ejector section was a 20-in.-diam exhaust plenum which contained two, 15- by 6-in. rectangular windows. Access to the centerbody drive motor, the centerbody position indicator, and the pressure sensing lines was obtained through the rectangular windows.

A remotely controlled valve was installed downstream of the exhaust plenum. The valve was used to increase or decrease the operating pressure ratio by varying exhaust pressure.

To simulate test cell cooling air, a 2-in.-diam secondary airflow duct was connected to the test cell as shown in Fig. 1. Secondary airflow was metered by a contoured nozzle having a minimum throat diameter of 1.25 in. and a nozzle exit area-to-nozzle throat area ratio (A_{ne}/A^*) of 2.917.

2.2 PRIMARY DRIVING NOZZLES

Two fixed-geometry primary driving nozzles (Fig. 2) having 36-deg total conical angles were used during this investigation. The first nozzle, which had a nozzle exit area-to-throat area ratio (A_{ne}/A^*) of 1.637 and an associated ejector area-to-throat area ratio (A_d/A^*) of 3.987, simulated a turbojet engine in an afterburning mode of operation. The second driving nozzle, which had an A_{ne}/A^* of 1.66 and an associated A_d/A^* of 5.756, corresponded to a turbojet at military power.

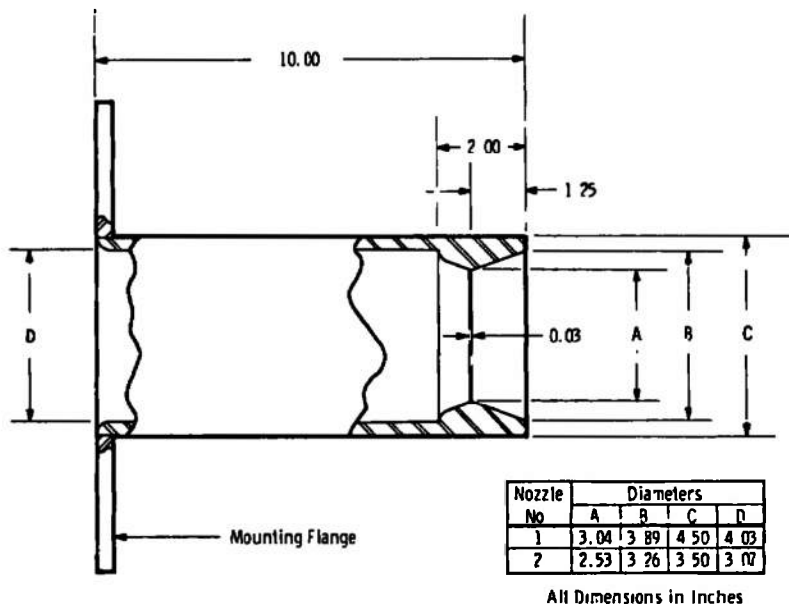


Figure 2. Primary nozzle details.

The primary nozzles were installed on the 10-in.-diam inlet duct inside and concentric with the test cell (Fig. 1) with the nozzle exit located 2.06 in. inside the ejector cylindrical inlet duct.

2.3 CONSTANT-AREA EJECTOR

The constant-area ejector (Fig. 3) was tested for performance comparison with the variable-area ejectors. The ejector was constructed by modifying a section of the variable-area ejector hardware. The variable-area hardware consisted of a 1-in.-long, 12.5-deg, half-angle converging conical inlet to the 6.07-in.-diam cylindrical duct, which was 8.63 in. in length; an 8-in.-long, 12.5-deg half-angle, diverging conical section; and a 12-in.-long, 10.2-in.-diam section. The constant-area ejector was constructed by adapting a 20.05-in.-long, 6.07-in.-diam insert, arranged as depicted in Fig. 3. The leading edge of the insert was tapered to match the 12.5-deg half-angle diverging section and was sealed by a silicon rubber pad. The cylindrical duct length-to-diameter ratio was 4.54, which was equivalent to that of each of the variable-area ejectors.

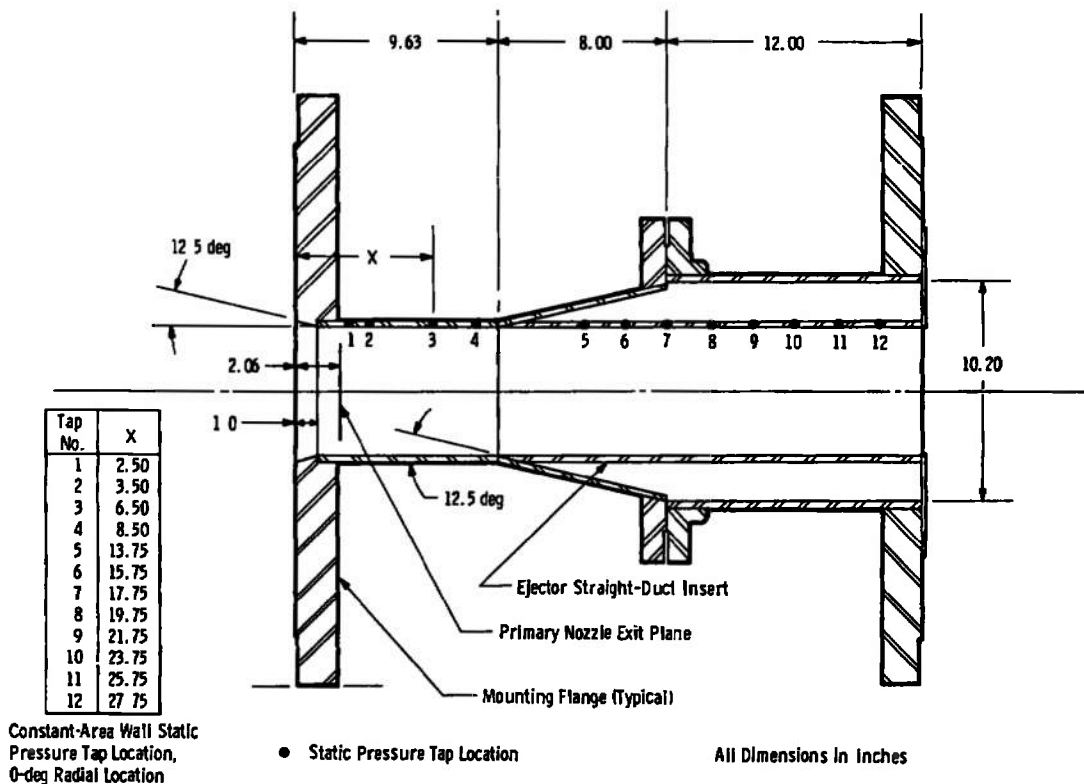


Figure 3. Details of constant-area ejector.

2.4 VARIABLE-AREA EJECTORS

Three variable-area ejectors were evaluated during this investigation (the double-angle centerbody, the triple-angle centerbody, and the single-angle centerbody) in an effort to optimize ejector performance.

The minimum area of each variable ejector configuration was varied by a centerbody positioning rod that was driven by a variable-speed electric motor located in the 20-in.-diam exhaust plenum (Fig. 1). Centerbody position was manually read from a pointer located in one of the windows in the exhaust plenum. The centerbody could be moved upstream or downstream as desired during testing.

2.4.1 Double-Angle Centerbody Ejector

The double-angle centerbody ejector (Fig. 4) consisted of the hardware used for the constant-area ejector excluding the insert and including the double-angle centerbody. The overall length-to-capture duct diameter ratio (L/D) of the ejector was 4.54.

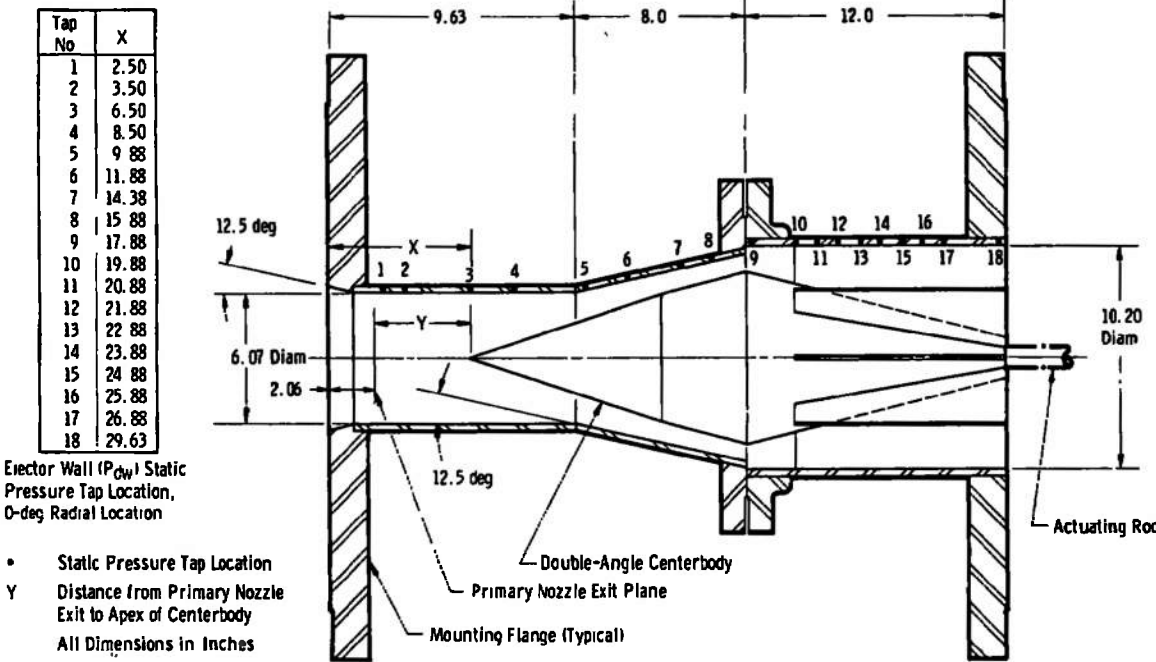
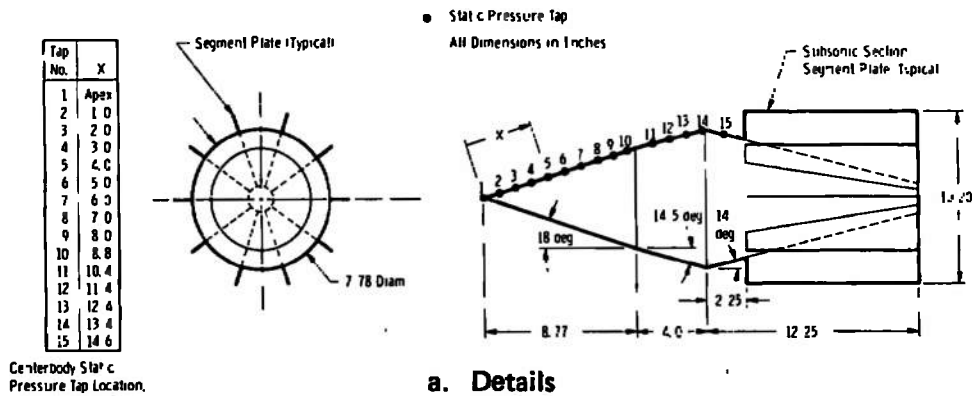


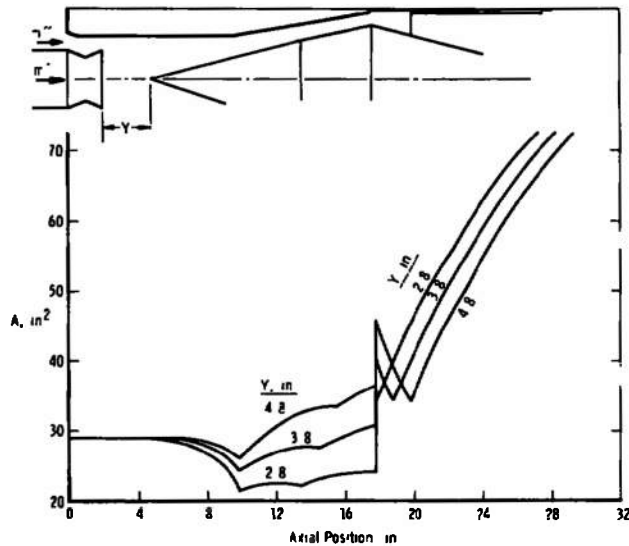
Figure 4. Variable-area ejector with double-angle centerbody.

The centerbody (Fig. 5a) had a spike half-angle of 18 deg, a truncated second half-angle of 14.5 deg, and a converging conical half-angle of 14 deg. Segment plates, which divided the converging section into 10 equally dimensioned passages, were installed to provide an improvement in ejector performance and as a device for positioning the centerbody in the ejector. The centerbody length was 25.02 in., and the maximum diameter was 7.78 in.

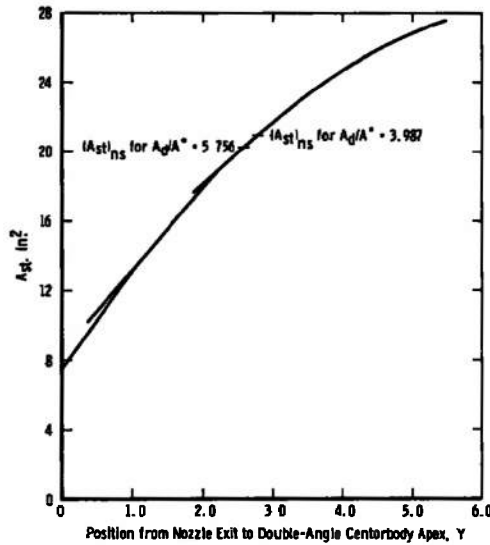


a. Details
Figure 5. Double-angle centerbody.

The double-angle centerbody configuration produced an axial variation in flow area as depicted in Fig. 5b and a second-throat area versus centerbody position shown in Fig. 5c. These flow areas are for the ideal case without boundary layer effect and with flow parallel to the duct wall. The points of double-value throat area occur when the second-throat area location shifts to either the duct angle change, the centerbody angle change, or the maximum diameter of the centerbody.



b. Flow area versus axial position
Figure 5. Continued.



c. Second-throat area versus centerbody position
Figure 5. Concluded.

2.4.2 Triple-Angle Centerbody Ejector

The triple-angle centerbody configuration (Fig. 6) resulted from modifying the apex of the double-angle centerbody configuration. The centerbody (Fig. 7a) was modified to have an apex half-angle of 12 deg, a truncated second half-angle of 25 deg, a truncated third half-angle of 14.1 deg, and an overall length of 24.55 in.

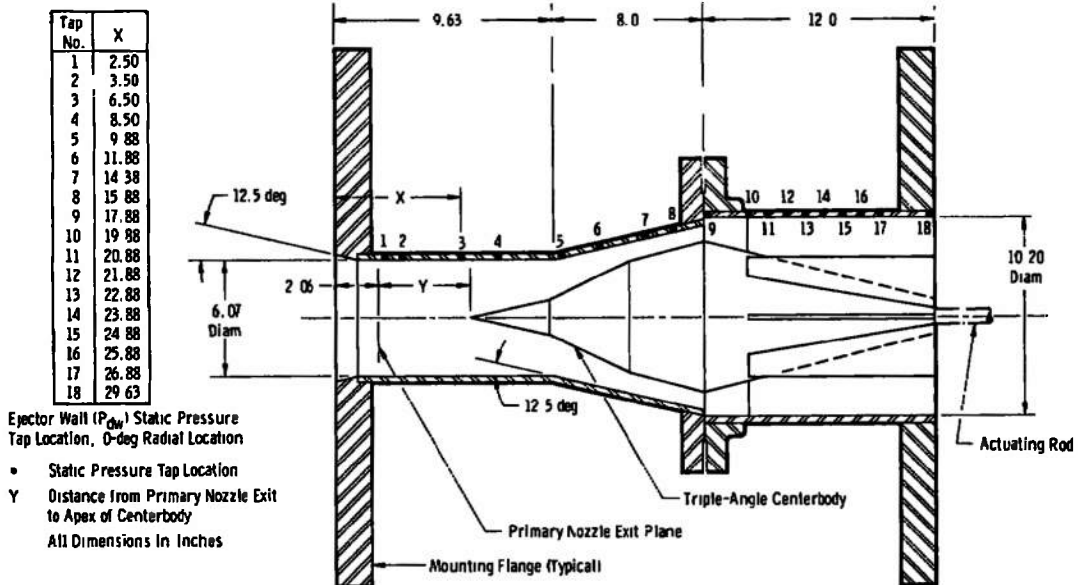
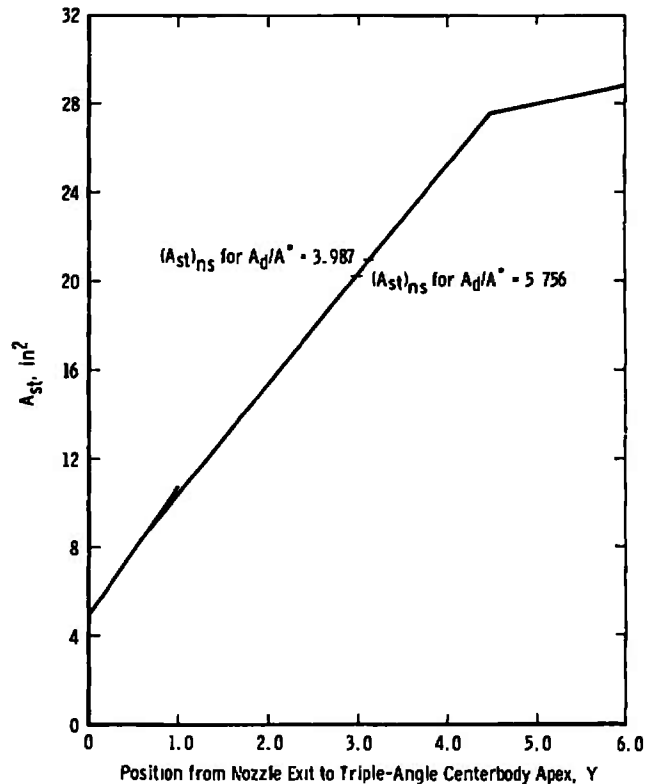


Figure 6. Variable-area ejector with triple-angle centerbody.



c. Second-throat area versus centerbody position
Figure 7. Concluded.

2.4.3 Single-Angle Centerbody Ejector

The single-angle centerbody ejector configuration (Fig. 8) consisted of a 6.07-in.-diam cylindrical capture duct 10 in. in length, an 8-deg half-angle truncated conical diverging section 13 in. long, a 10.2-in.-diam cylindrical subsonic section 6.63 in. long, and a blunt single-angle centerbody. An effective ejector length-to-capture duct diameter ratio (L/D) of 4.54 was maintained.

The centerbody (Fig. 9a) had a single 12-deg half-angle spike with a nose radius of 0.50 in. The spike was 11.87 in. long with a major diameter of 6.0 in. and a cylindrical aft section 6.0 in. in diameter and 4 in. long. A centerbody support spider retained the centerbody on the centerline of the ejector and allowed the centerbody to be positioned by movement of the positioning rod.

The single-angle centerbody configuration produced an axial variation in flow area as shown in Fig. 9b and a second-throat area versus centerbody position as shown in Fig. 9c.

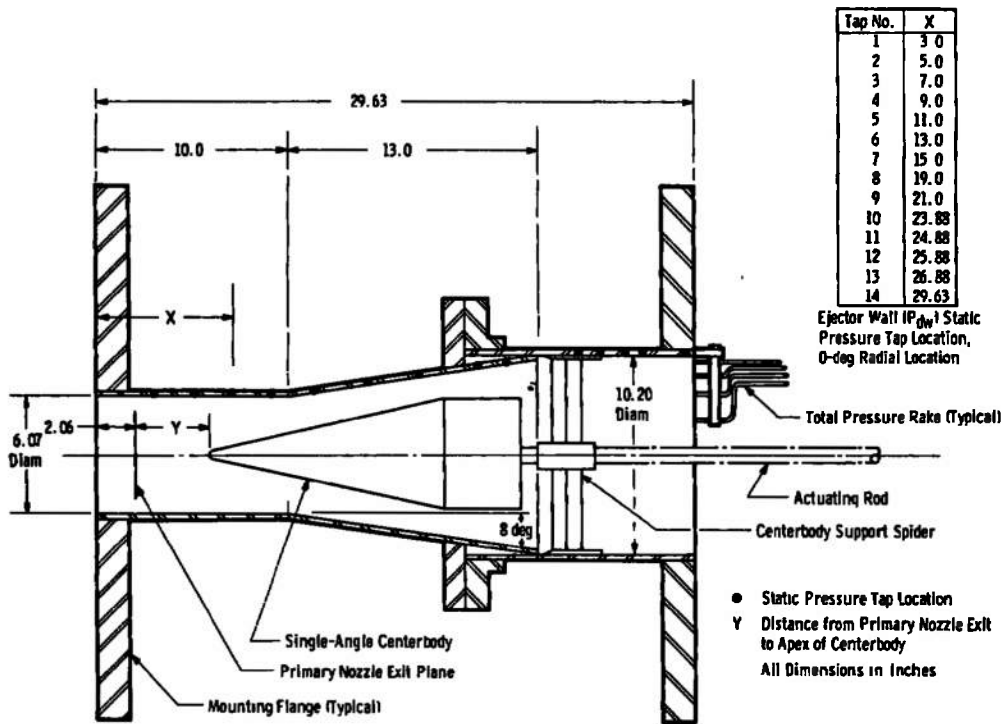
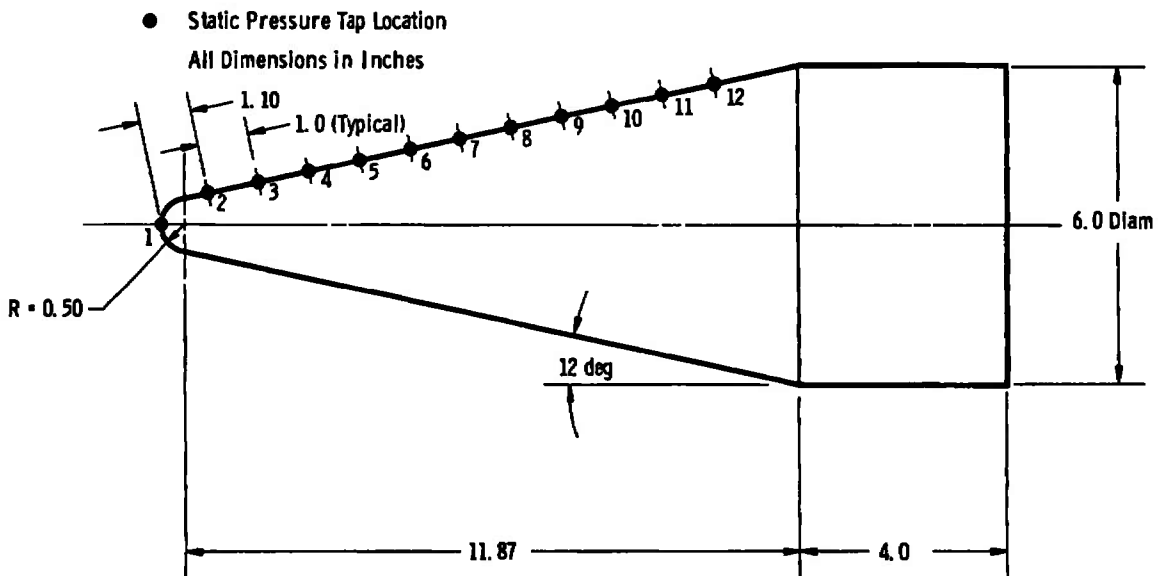
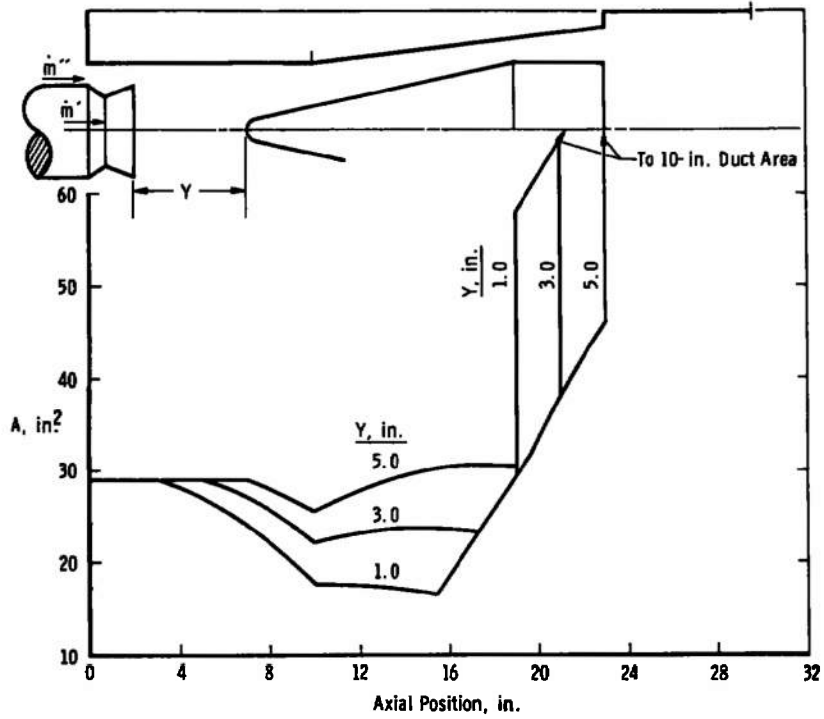


Figure 8. Variable-area ejector with single-angle centerbody.

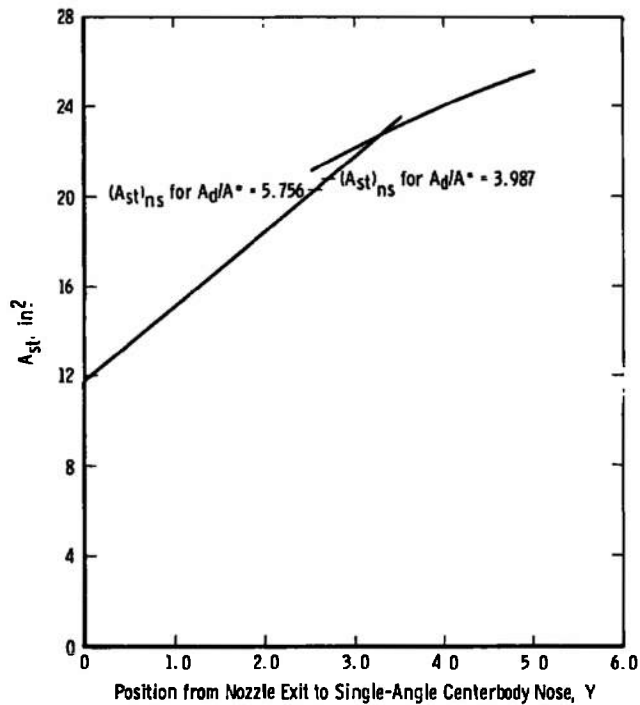


a. Details

Figure 9. Single-angle centerbody.



b. Flow area versus axial position



c. Second-throat area versus centerbody position
Figure 9. Concluded.

2.5 VENTURI

The venturi installation was arranged as shown in Fig. 10. The venturi was located in standard flanged ducting with four pitot pressure tubes in the 10-in. inlet duct and two flow-straightening screens providing 40-percent blockage in the inlet plenum. The screen produced a constant pressure profile on the 9-tube pitot rake shown in Fig. 11, that was located near the inlet of the venturi. The venturi exit plane was fitted with a 15-tube pitot pressure rake depicted in Fig. 12. Static pressure was measured on the duct near the exit plane of the venturi.

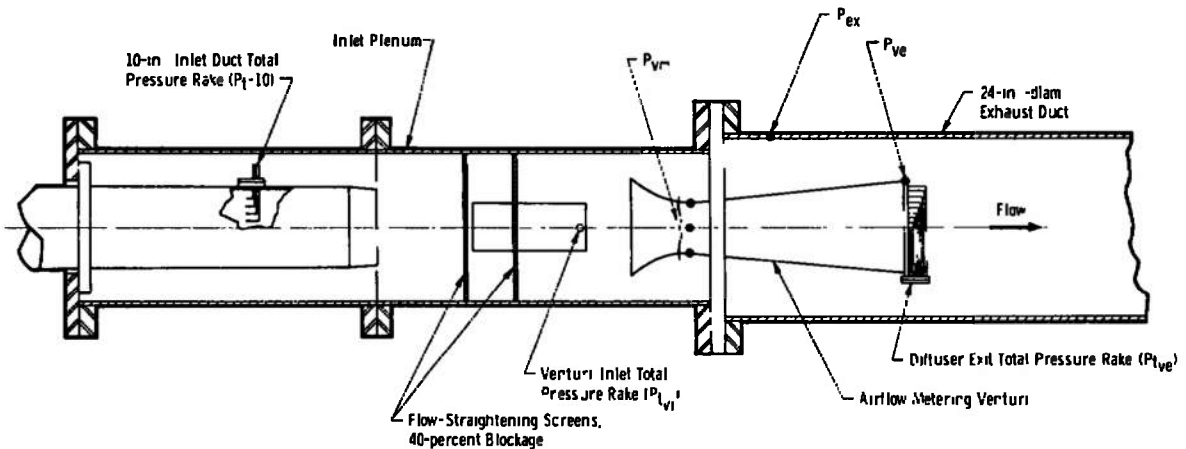


Figure 10. Test section with typical venturi installation.

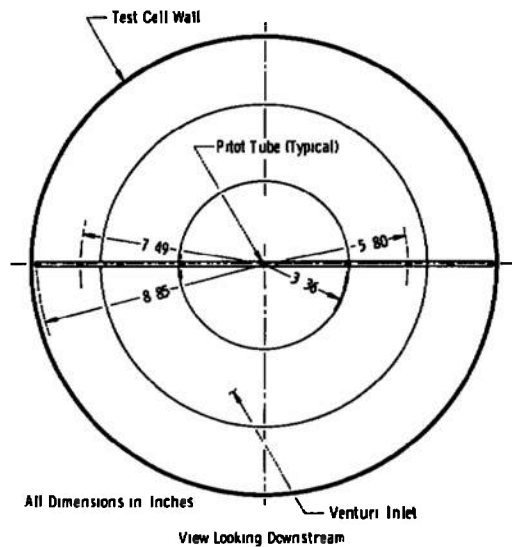


Figure 11. Venturi inlet total pressure probe arrangement.

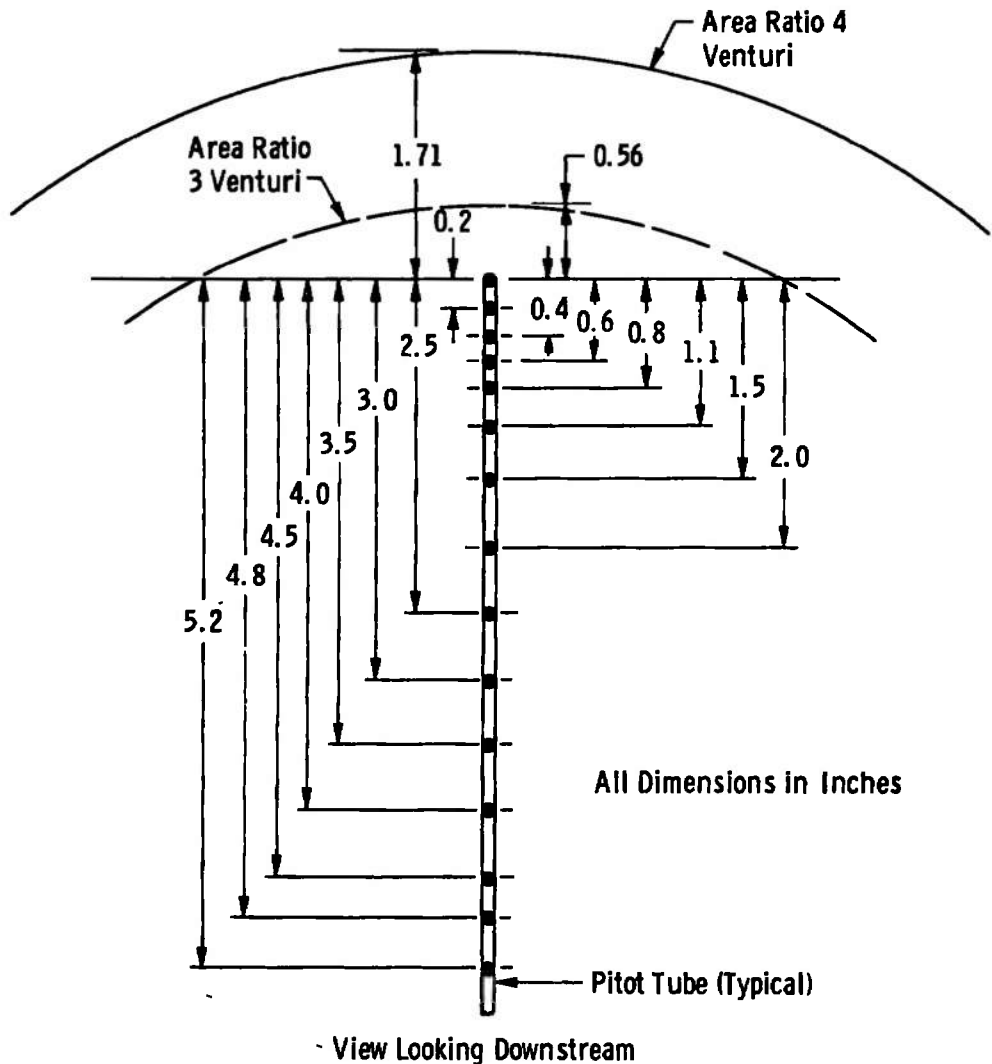
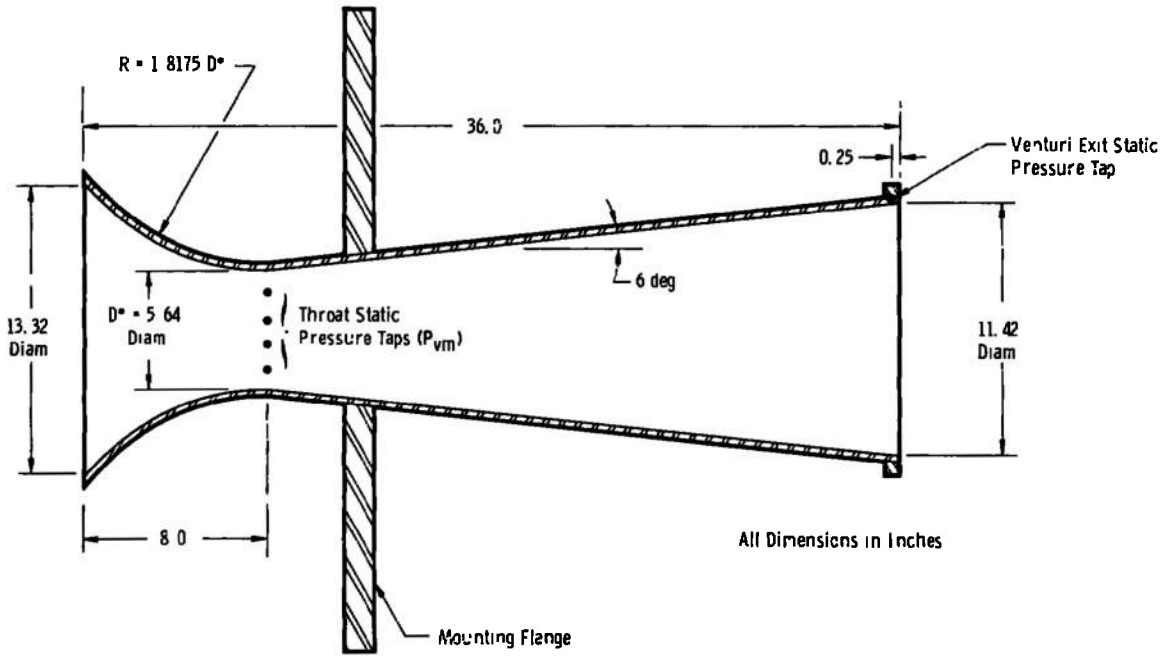
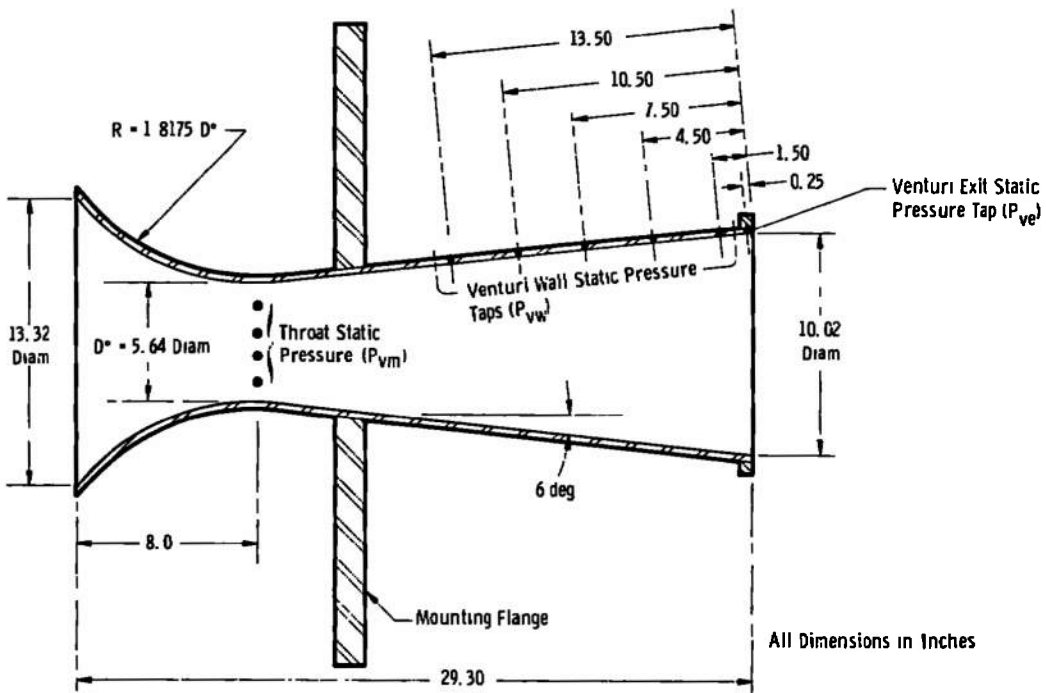


Figure 12. Venturi exit total pressure probe arrangement.

The dimensions of the venturis are shown in Fig. 13. Both venturis were constructed of mild steel mounted on a standard 1.25-in.-thick by 38.75-in.-diam flange with a drilled 24-in.-diam mounting bolt circle. The throat diameters (D^*) are both 5.64 in. with exit diameters of 11.42 and 10.02 in., resulting in venturi exit-to-throat area ratios (A_{ve}/A^*) of 4.10 and 3.16, respectively. The $A_{ve}/A^* = 3.16$ venturi was obtained by shortening the length of the $A_{ve}/A^* = 4.10$ venturi by 6.7 in. The inlet of the venturi was designed with a 1.8175 D^* radius to the point of tangency with the 6-deg half-angle conical diverging section. The machined surface of the venturi was painted with a surface finish over paint of 30 to 50 microinches.



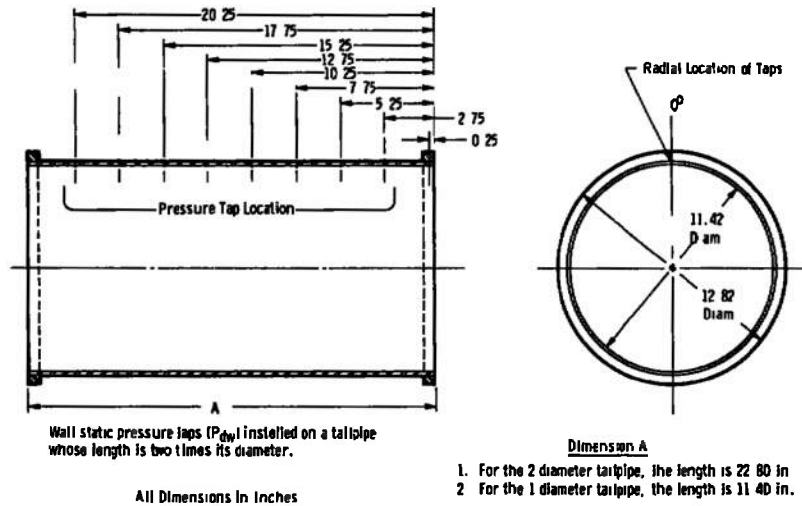
a. $A_{v0}/A^* = 4.10$



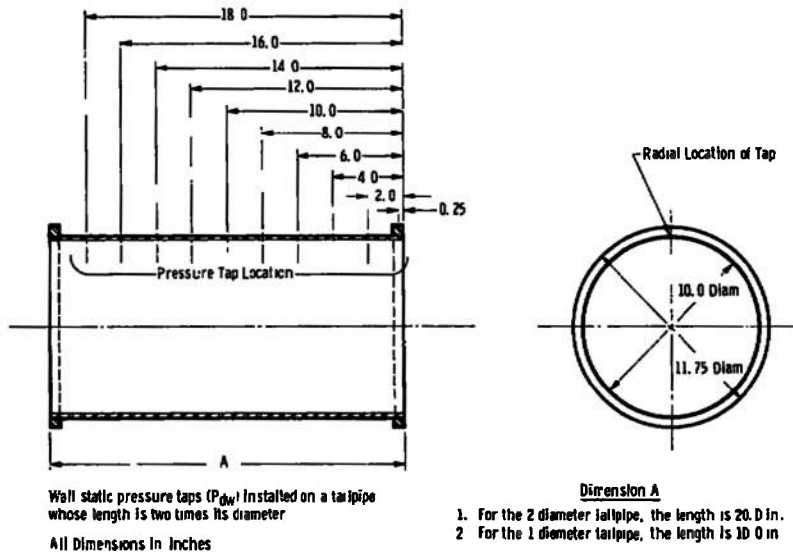
b. $A_{v0}/A^* = 3.16$

Figure 13. Details of air-metering venturis.

The venturi was instrumented at the throat (P_{vm}), along the conical wall (P_{vw}), and at the exit plane (P_{ve}) with drilled and tapped static pressure probes. The tailpipes, illustrated in Fig. 14, were made of standard mild steel ducting rolled to the desired diameter. The static pressure probes were arranged as shown in these illustrations. The tailpipes were fitted with bolt mounts on the stiffening rings, allowing the length to be varied by connecting the desired tailpipe. A typical tailpipe configuration is presented in Fig. 15.



a. $A_{ve}/A^* = 4.10$



b. $A_{ve}/A^* = 3.16$

Figure 14. Details of diffuser tailpipe.

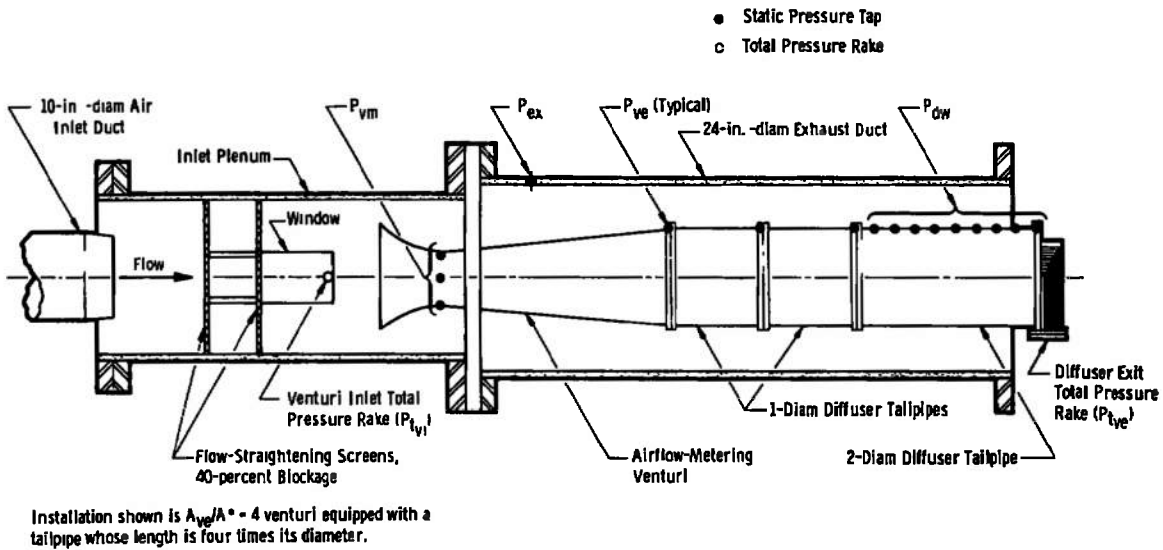


Figure 15. Typical venturi installation with tailpipe.

2.6 INSTRUMENTATION

Static and total pressure parameters were measured by a 120-in. manometer board filled with mercury and recorded on 70-mm film. The mercury had a specific gravity of approximately 13.5305 at 80°F. The accuracy of the manometer board is believed to be excellent because (1) the mercury tubes were referenced to atmosphere and the data taken from the barometer were used in reducing the manometer board data. The range of the barometer was 28- to 31-in. HgA with a calibrated maximum deviation of ± 0.01 -in. HgA, and (2) a vacuum check was taken before testing and at an interval during testing to ensure that the manometer board and pressure lines contained no leaks.

Centerbody position was measured by a mechanical pointer and scale divided into 0.10-in. increments and was recorded manually. Accuracy of the position indicator was believed to be ± 0.05 in.

Four pitot tubes positioned on equal areas were located in the 10-in.-diam primary air supply duct for measuring air inlet total pressure (P_t').

A single pitot tube located on the centroid of the duct area in the secondary air duct upstream of the secondary air-metering venturi sensed the secondary air total pressure (P_t'').

Four rakes (Fig. 16), containing four pitot tubes each, were installed at the ejector exits for measuring the total pressures.

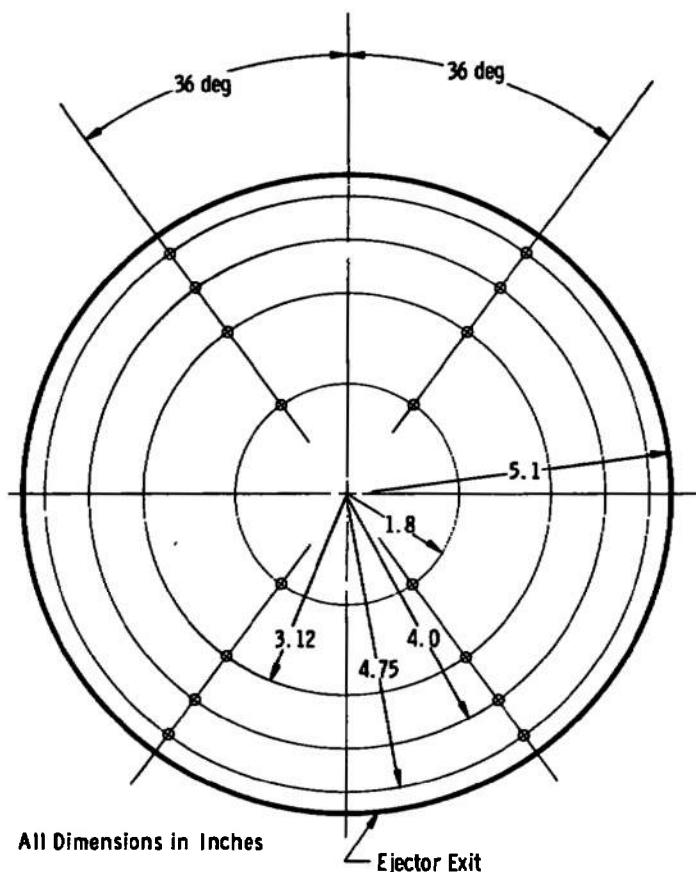


Figure 16. Ejector exit total pressure probe arrangement.

Ejector wall static pressure taps (P_{dw}) locations are shown in Figs. 3, 4, 6, and 8, and the ejector centerbody surface static pressure taps are shown in Figs. 5a, 7a, and 9a, where "X" represents the axial location of the taps.

The axial positions of test cell and exhaust static pressure taps are shown in Fig. 1.

3.0 PROCEDURE

The primary nozzle inlet conditions, mainly stagnation pressure P_t' , were held constant for each test. The secondary nozzle inlet parameters were varied depending on the \dot{m}''/\dot{m}' ratio desired: 0, 5,

10, or 15 percent. The exhaust pressure (P_{ex}) for the system was adjusted to the desired value during each test by throttling through the exhaust isolation valve.

The test was initiated according to the following procedure:

1. The exhaust valve was opened and the exhaust system evacuated the test cell;
2. A vacuum check was conducted to check for leaks in hardware and instrumentation; and
3. The air supply valve was opened and the air supply pressure was adjusted to 20 psia for the ejector or 8 psia for the venturi tests.

The centerbody was then moved forward to the axial position at which cell pressure (P_c) was first observed to fluctuate and/or increase in value. The exhaust pressure was then increased in small increment, and data were recorded. These procedures were performed for each \dot{m}''/\dot{m}' ratio established. The procedures for testing the constant-area ejector and the venturi were the same with the exception of the centerbody movement.

4.0 RESULTS AND DISCUSSION

4.1 GENERAL INFORMATION

An explanation of ejector-diffuser performance parameter terminology is necessary to the understanding of terms used in this discussion. Figure 17 shows a typical ejector performance curve. The primary nozzle flow accelerates until it becomes supersonic throughout the diverging section of the nozzle and the cylindrical inlet or capture duct, which effects a decrease in the value of cell pressure by entrainment mixing until a minimum cell pressure ratio (P_c/P_t) is obtained. The minimum cell pressure ratio is shown as point (c). The operating pressure ratio (P_{ex}/P_t) necessary to obtain this minimum cell pressure ratio is depicted as point (a) in Fig. 17, and the ejector is considered started. Once steady-state conditions exist on the line of minimum cell pressure, it may be possible to increase the operating pressure ratio (P_{ex}/P_t) to a point greater than the starting value by increasing P_{ex} until P_c begins to change. This is depicted by point (b) and is the maximum operating pressure ratio. The maximum rise ratio (P_{ex}/P_c) also occurs at this point.

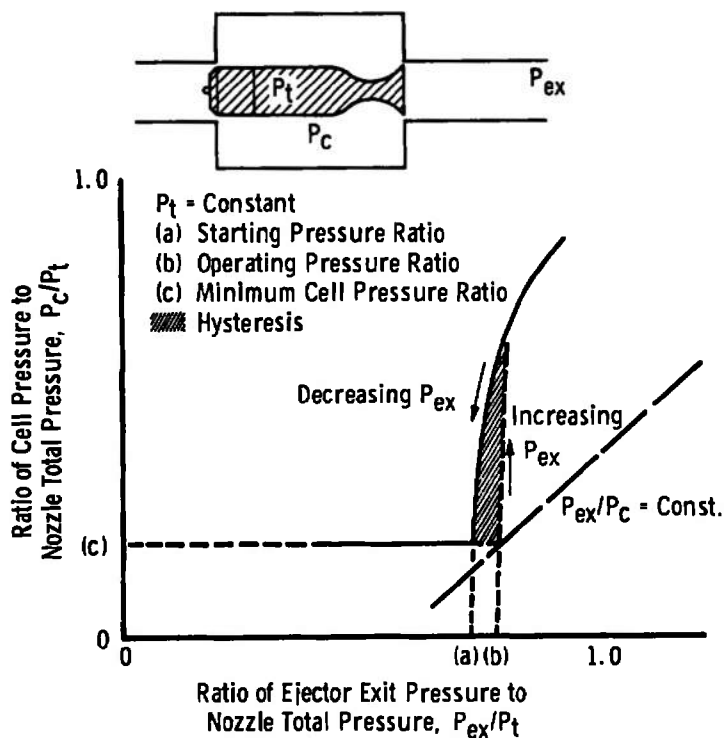


Figure 17. Typical ejector characteristics.

Considerable effort has been made to develop theoretical methods for ejector design. At present, all methods used tend to be semi-empirical and require the use of a digital computer. The state-of-the-art method of second-throat ejector design (presented in Refs. 1 and 2) using a one-dimensional application of the conservation analysis employing empirical correction factors is generally accepted as a reasonable performance estimation. The second-throat area for the condition of no secondary flow $[(A_{st})_{ns}]$ is designed using the equation:

$$(A_{st})_{ns} = \frac{A^*}{(P_{t_2}/P_{t_1})_{ns}} \quad (\text{from Ref. 2})$$

where $(P_{t_2}/P_{t_1})_{ns}$ is the total pressure loss of a normal shock corresponding to the A_d/A^* of the ejector from the isentropic gas tables. These values of second-throat area are shown in Figs. 5c, 7c, and 9c.

The theory used to evaluate ejector performance and static pressure rise is from Ref. 2 and is compiled with the aid of a digital computer.

4.2 CONSTANT-AREA EJECTOR

The constant-area ejector illustrated in Fig. 9 was used for performance comparison with the centerbody configurations. The constant-area ejector performance is presented in Figs. 18a and b for the respective capture duct to nozzle throat area ratios (A_d/A^*) of 3.987 and 5.756. The latter ratio represents turbojet operation at military power without afterburning, whereas the former simulates augmented power.

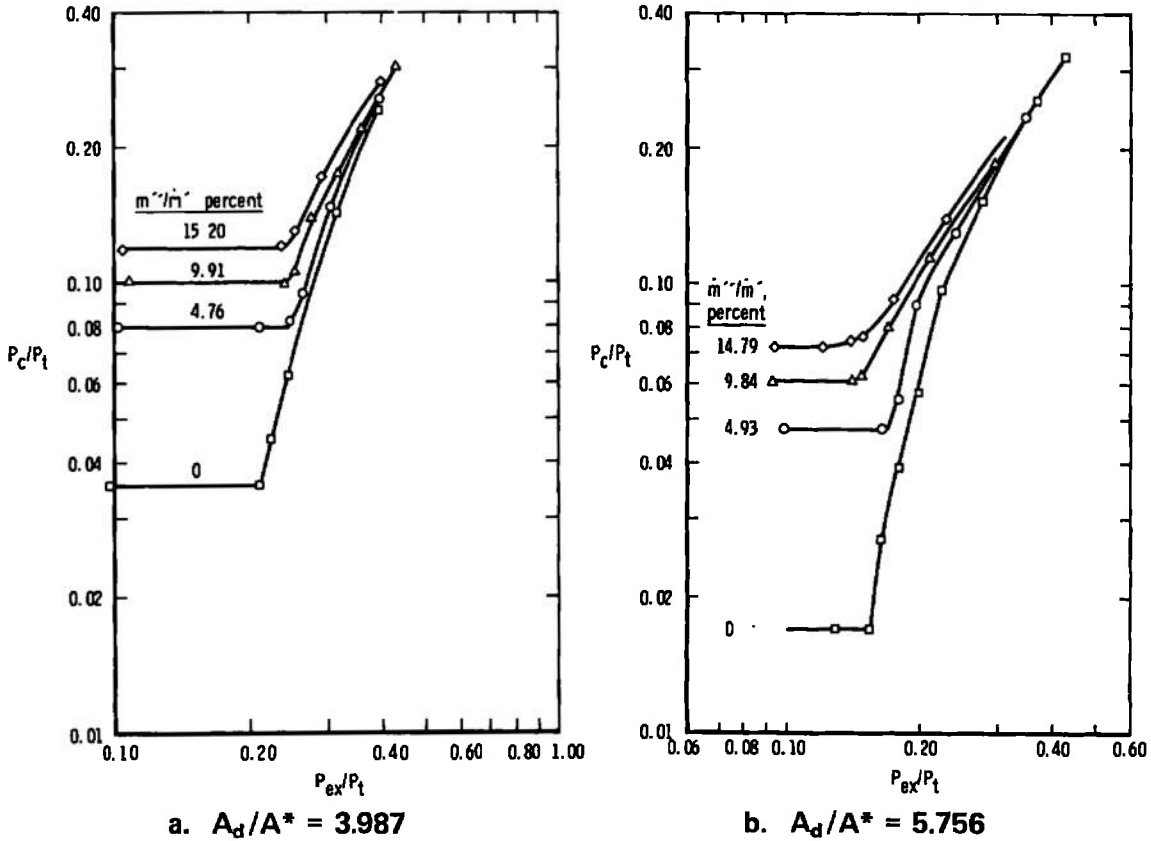


Figure 18. Constant-area ejector characteristic.

4.3 THE DOUBLE-ANGLE CENTERBODY VARIABLE-AREA EJECTOR

The double-angle centerbody configuration illustrated in Figs. 4 and 5a showed difficulty in "starting." The axial position of the centerbody (Y), at which cell pressure was affected, was 4.30 in. This can be seen by observing Fig. 19. The second-throat area in Fig. 5c corresponding to this position was discovered to be larger than that corresponding to the normal shock second-throat area ($A_{st})_{ns}$. This large second-throat adversely affects performance.

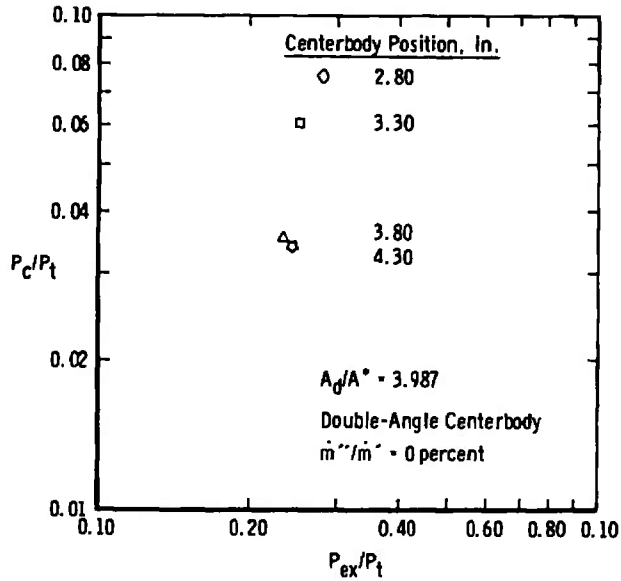


Figure 19. Double-angle centerbody variable-area ejector starting characteristics.

Inspection of Fig. 20 reveals that the static pressure rise for the axial distance was greater for the centerbody-type ejector. This shows some definite advantage to the more complex system. Thus, the double-angle centerbody configuration showed a definite increase in the diffusion rate over that of the constant-area ejector.

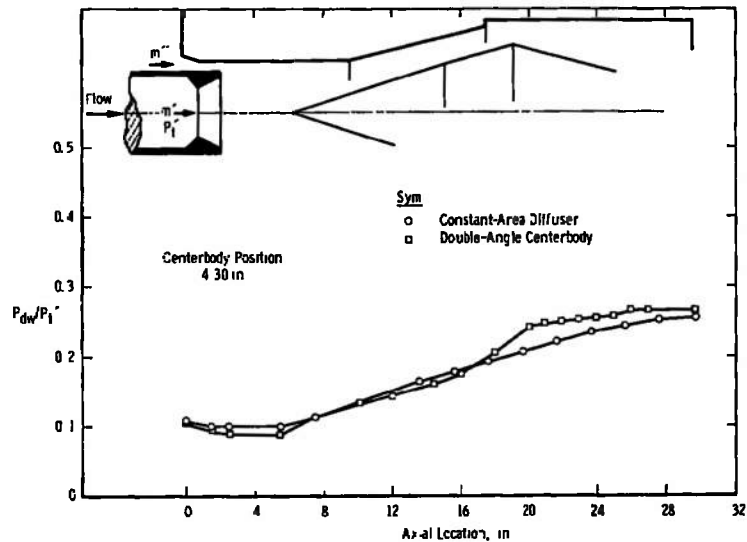
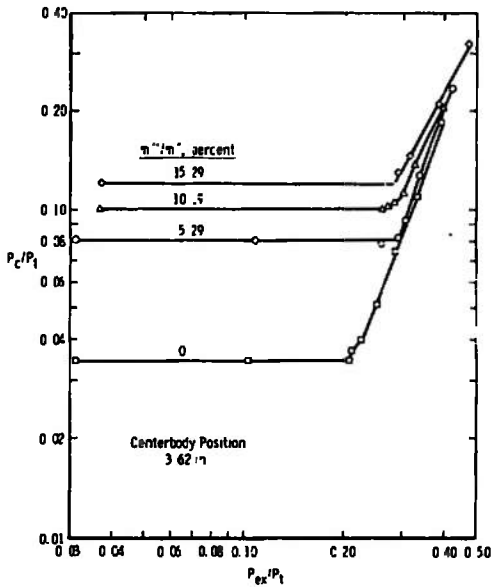


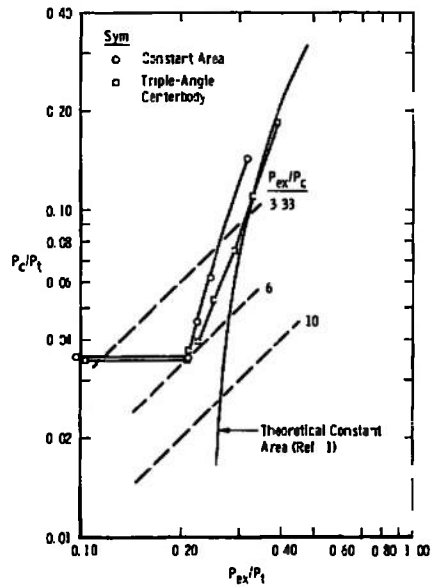
Figure 20. Double-angle centerbody variable-area ejector.

4.4 THE TRIPLE-ANGLE CENTERBODY VARIABLE-AREA EJECTOR

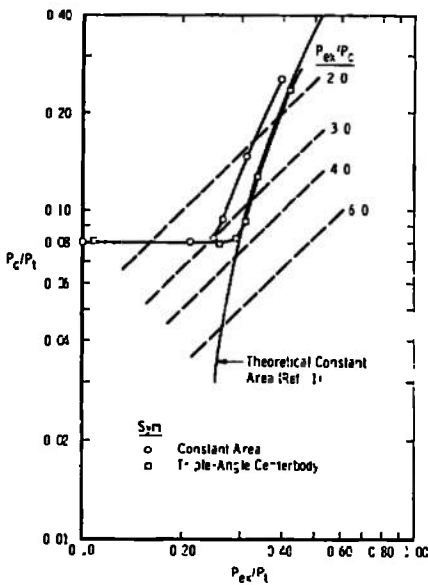
The triple-angle centerbody configuration presented in Figs. 6 and 7a produced somewhat better performance than the constant-area ejector. The performance of this configuration appears in Fig. 21 for A_d/A^* of 3.987 and in Fig. 22 for A_d/A^* of 5.756.



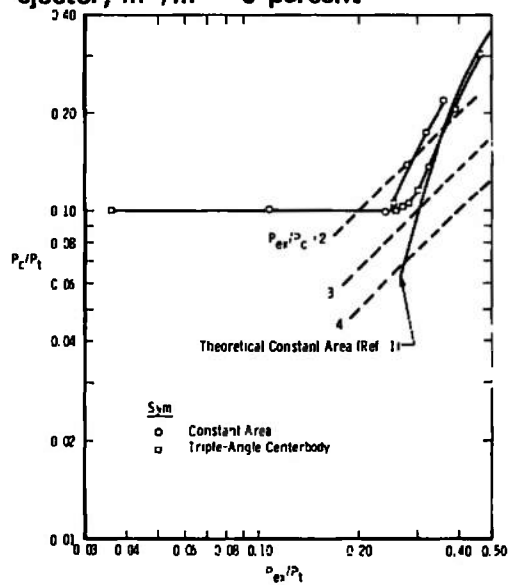
a. Overall performance



b. Performance compared with constant-area ejector, $\dot{m}''/\dot{m}' = 0$ percent



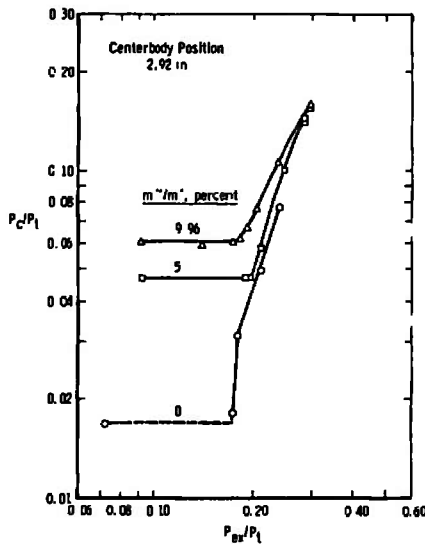
c. Performance compared with constant-area ejector, $\dot{m}''/\dot{m}' = 5$ percent



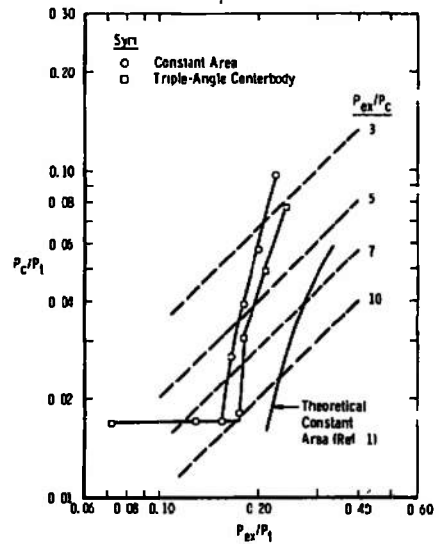
d. Performance compared with constant-area ejector, $\dot{m}''/\dot{m}' = 10$ percent

Figure 21. Triple-angle centerbody variable-area ejector, $A_d/A^* = 3.987$.

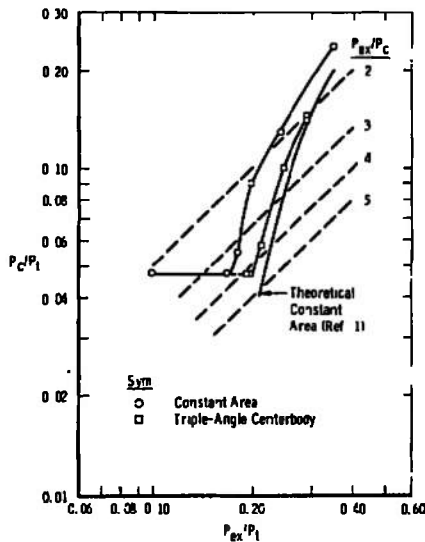
The ejector performance characteristics are shown to be better than those of the constant area ejector. The rise ratio improvements of the $A_d/A^* = 3.987$ configuration were 1.2, 16.5, and 10.8 percent for \dot{m}''/\dot{m}' of 0, 5, and 10 percent, respectively. For $A_d/A^* = 5.756$, the respective rise ratio improvements were 5.3, 14.3, and 25.3 percent for \dot{m}''/\dot{m}' of 0, 5, and 10 percent.



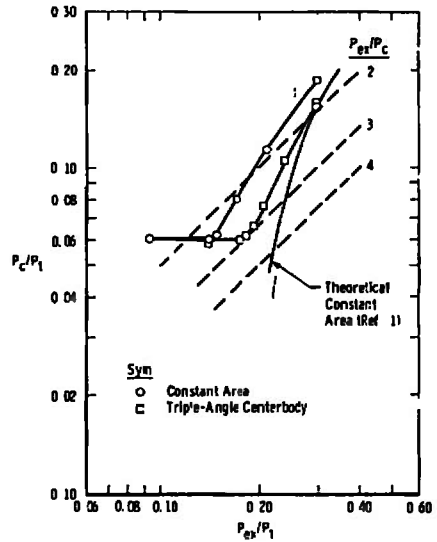
a. Overall performance



b. Performance compared with constant-area ejector, $\dot{m}''/\dot{m}' = 0$ percent



c. Performance compared with constant-area ejector, $\dot{m}''/\dot{m}' = 5$ percent



d. Performance compared with constant-area ejector, $\dot{m}''/\dot{m}' = 10$ percent

Figure 22. Triple-angle centerbody variable-area ejector, $A_d/A^* = 5.756$.

The triple-angle centerbody configuration allowed a greater operating range than the double-angle type. The starting characteristics were considerably more desirable. The ejector would start at 3.22 centerbody position, which is nearer the ideal contraction ratio. The diffusion rate increase is shown in Fig. 23. The static pressure rise on the centerbody to a segment on the variable-area diffuser where the flow area becomes nearly constant was as depicted by a line from 1 to 2 in Fig. 7b. The pressure rise from this point on is much greater than the pressure rise for the constant-area ejector.

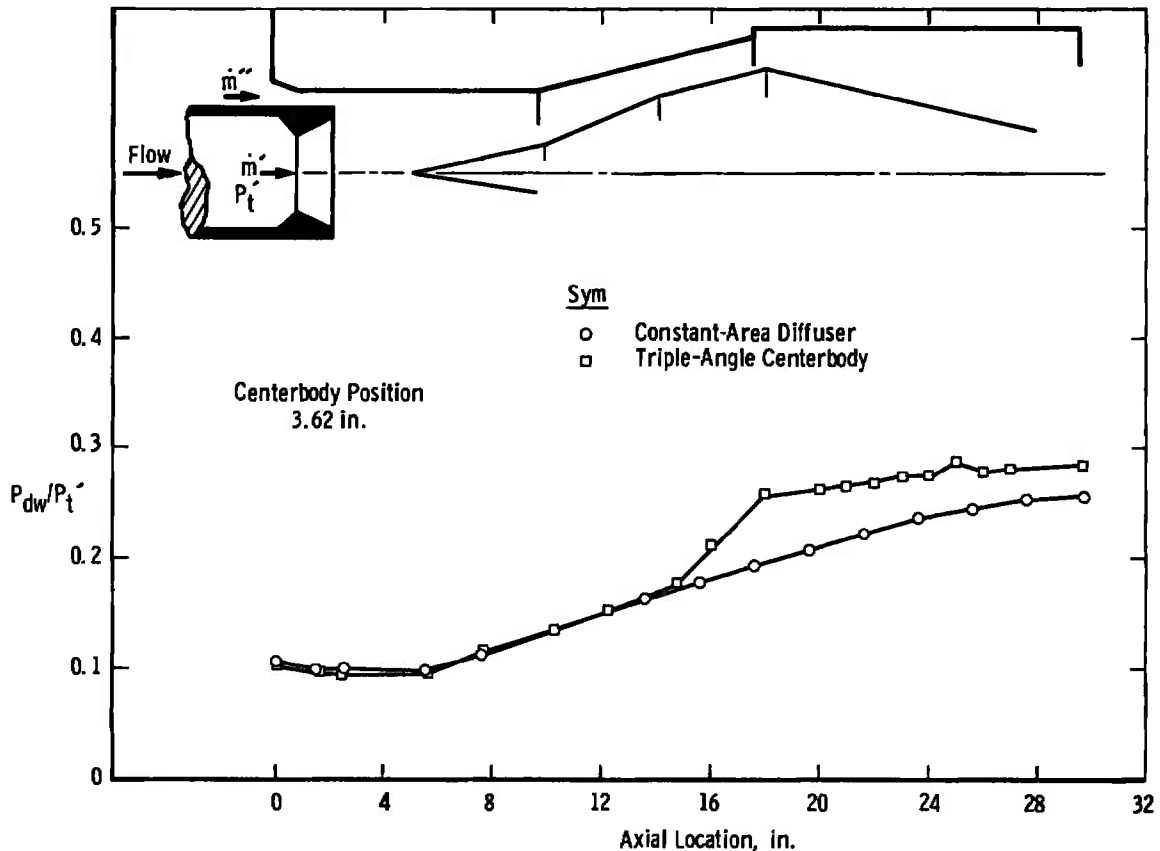
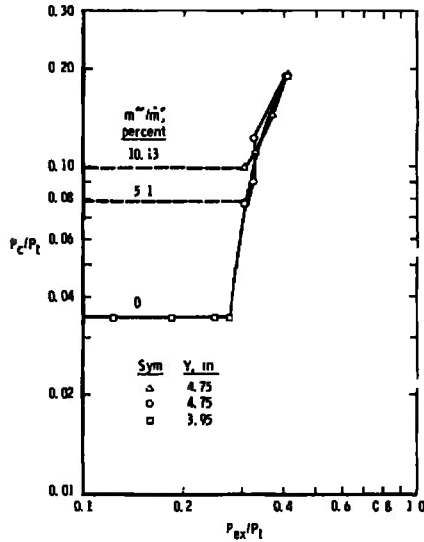


Figure 23. Triple-angle centerbody variable-area ejector axial static pressure, $\dot{m}''/\dot{m}' = 10$ percent, $A_d/A^* = 3.987$.

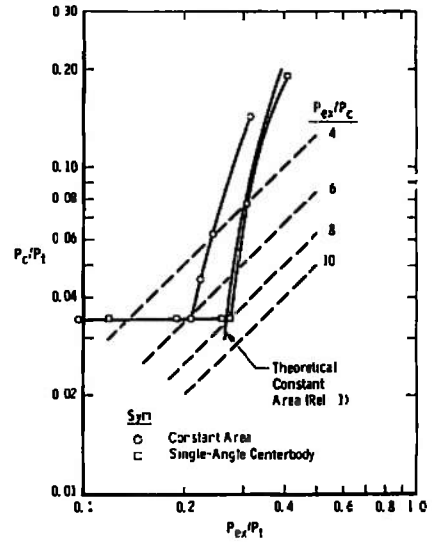
This configuration, although it allowed much greater performance, was undesirable because of the complex shape which would create difficult problems in an actual application at gas temperatures of 3500°F. Therefore, the centerbody was modified to a single-angle configuration.

4.5 THE SINGLE-ANGLE CENTERBODY VARIABLE-AREA EJECTOR

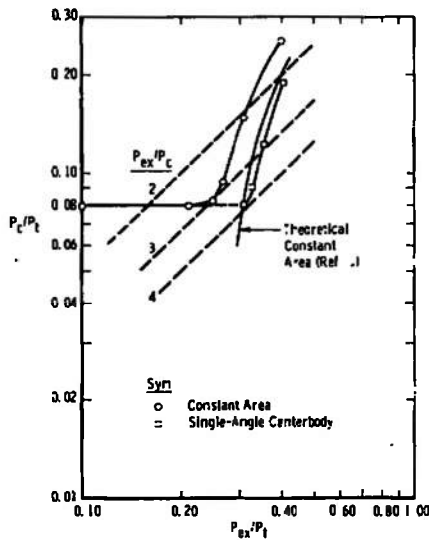
The single-angle centerbody configuration depicted in Figs. 8 and 9a produced the best results of the configurations tested. The ejector performance is presented in Fig. 24 for $A_d/A^* = 3.987$ and in Fig. 25 for $A_d/A^* = 5.756$.



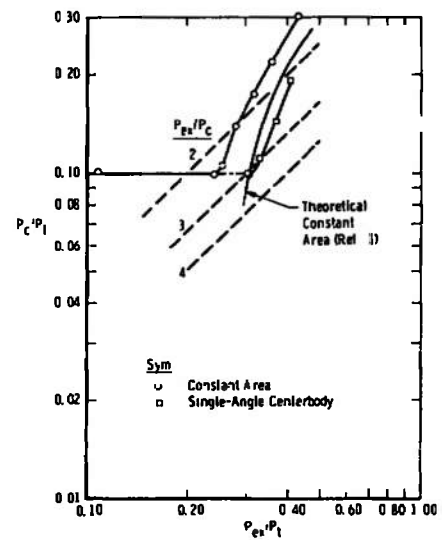
a. Overall performance



b. Performance compared with constant-area ejector, $m''/m' = 0$ percent



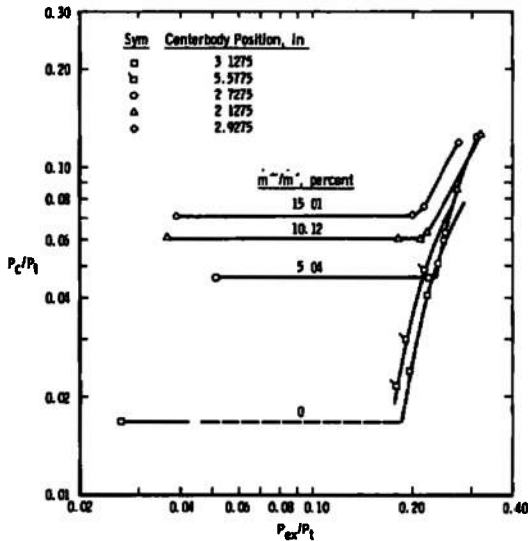
c. Performance compared with constant-area ejector, $m''/m' = 5$ percent



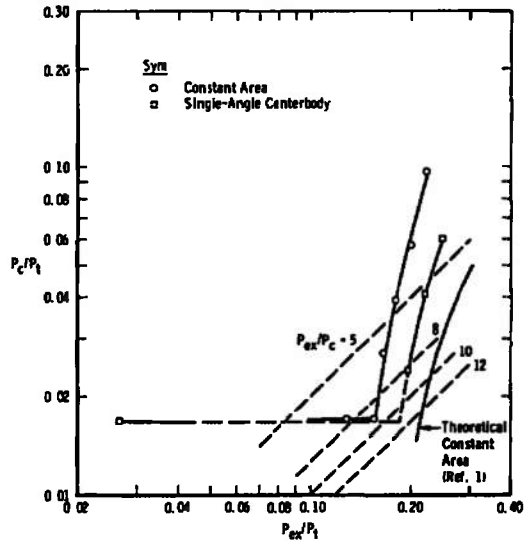
d. Performance compared with constant-area ejector, $m''/m' = 10$ percent

Figure 24. Single-angle centerbody variable-area ejector, $A_d/A^* = 3.987$.

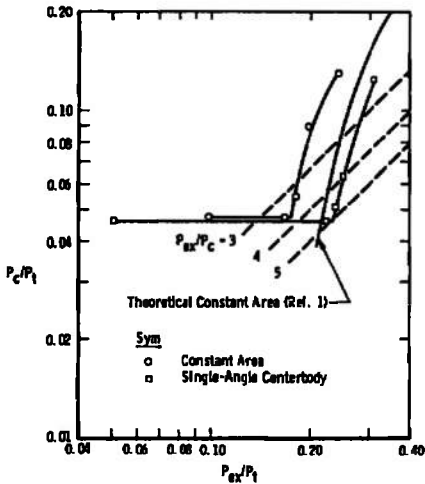
The performance is shown to be considerably better than the constant area ejector. The single-angle centerbody configuration improved the rise ratio in comparison to the constant-area ejector by 31.4, 24.4, and 27.3 percent for $A_d/A^* = 3.987$ and $\dot{m}''/\dot{m}' = 0, 5, \text{ and } 10$ percent, respectively. For $A_d/A^* = 5.756$, the respective rise ratio improvements were 34.5 and 46.5 percent for $\dot{m}''/\dot{m}' = 5$ and 10 percent and a projected improvement of 19.8 percent for $\dot{m}''/\dot{m}' = 0$ percent.



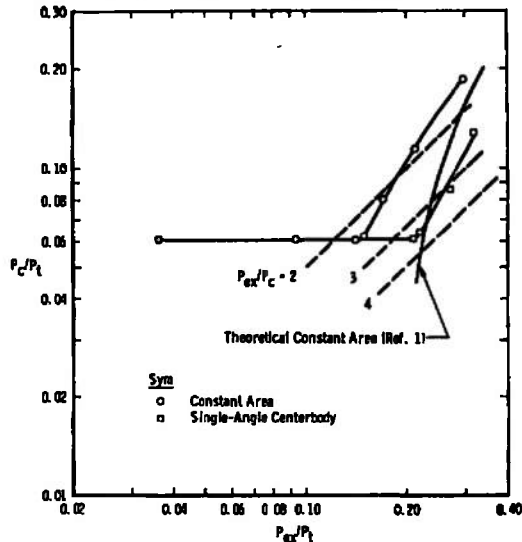
a. Overall performance



b. Performance compared with constant-area ejector, $\dot{m}''/\dot{m}' = 0$ percent



c. Performance compared with constant-area ejector, $\dot{m}''/\dot{m}' = 5$ percent



d. Performance compared with constant-area ejector, $\dot{m}''/\dot{m}' = 10$ percent

Figure 25. Single-angle centerbody variable-area ejector, $A_d/A^* = 5.756$.

The operating pressure ratio of the single-angle centerbody configuration with $A_d/A^* = 3.978$ and no secondary flow exceeded that of constant-area ejector by 30 percent. The ejector under those conditions started easily at the 4.75-in. position. The position was not varied to locate the optimum position for no secondary flow because of the limitation in centerbody movement.

The variation in wall static pressure rise ratio per unit length is depicted in Fig. 26. The centerbody configuration effects an appreciable improvement in the rate of diffusion over that of the constant-area ejector for 10-percent secondary flow.

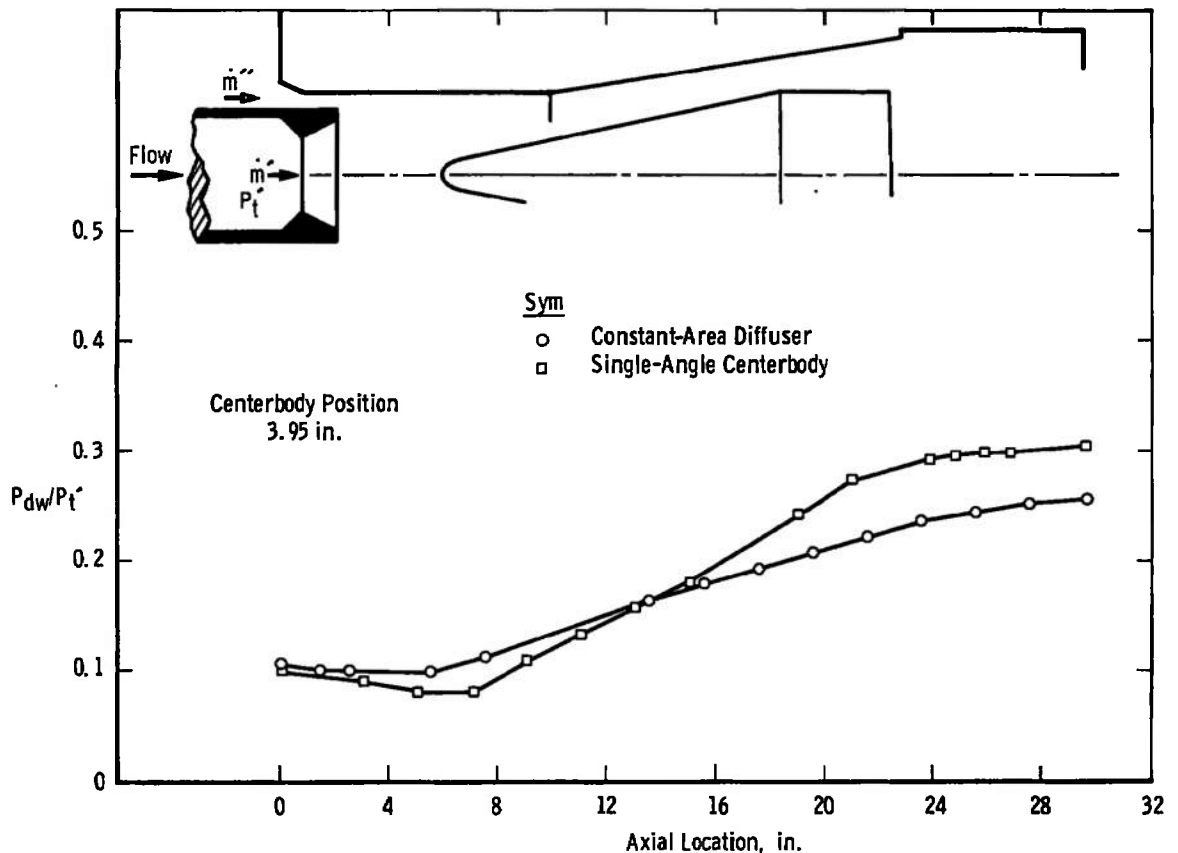


Figure 26. Single-angle centerbody variable-area ejector axial static pressure, $\dot{m}''/\dot{m}' = 10$ percent, $A_d/A^* = 3.987$.

The simpler design and improved performance provided insight for more testing that produced several unforeseen results.

4.6 THE OPTIMUM POSITION IMPROVEMENT

Figure 25a, in addition to showing the performance for all mass flow rates for $A_d/A^* = 5.756$, presents the off-optimum centerbody position in comparison with the optimum position for zero secondary flow. The flagged symbols are for the 5.58-in. position, while the unflagged symbols are for the 3.13-in. position. The contraction ratio (A_{st}/A_d) difference is 19.3 percent. This shows that the best performance is obtained for the smallest second-throat area that will maintain the minimum cell pressure ratio.

4.7 TEST CELL PRESSURE CONTROL

Test cell pressure was controlled between the minimum attainable by the installation and any desired value up to and including the ejector driving gas total pressure. The control was accomplished by throttling the flow through the ejector second-throat whose area was varied from the maximum obtainable to zero (throat completely blocked) by moving the centerbody. The pressure transient occurred in a smooth manner, and the cell pressure was stable at all pressure levels tested. These test cell pressure transients were conducted with the exhaust system pressure held constant at its minimum value (less than 1.0 psia). Therefore, the variable-area exhaust gas ejector may be used in ground test facilities to establish the transient altitude test requirements of jet propulsion systems; it may also be used to maintain sea-level static pressure in the test cell during propulsion system operation at all power settings.

4.8 EFFECT OF CENTERBODY POSITION FOR AN UNSTARTED PRESSURE RATIO

An interesting experimental result is depicted in Fig. 27 which is the ejector performance characteristic for $A_d/A^* = 5.756$ and $\dot{m}''/\dot{m}' = 5$ percent. The ejector performance was verified at a given centerbody position (square symbols), after which the centerbody was translated to decrease the second-throat area. The value of cell pressure decreased in a quasi-steady-state controllable manner as the centerbody was moved forward. When the centerbody position was reached at which test cell pressure attained a minimum value, the performance data were recorded. A 29.8-percent improvement in static pressure rise ratio (P_{ex}/P_c) resulted from the establishment of the optimum second-throat area. Thus, as is shown experimentally, a variable area ejector permits the optimization of performance through the establishment of the optimum second-throat area at every operating

condition, which effects an extension of facility performance capability. The conservation analysis presented in Ref. 1, produced results that compared favorably with the experimental values.

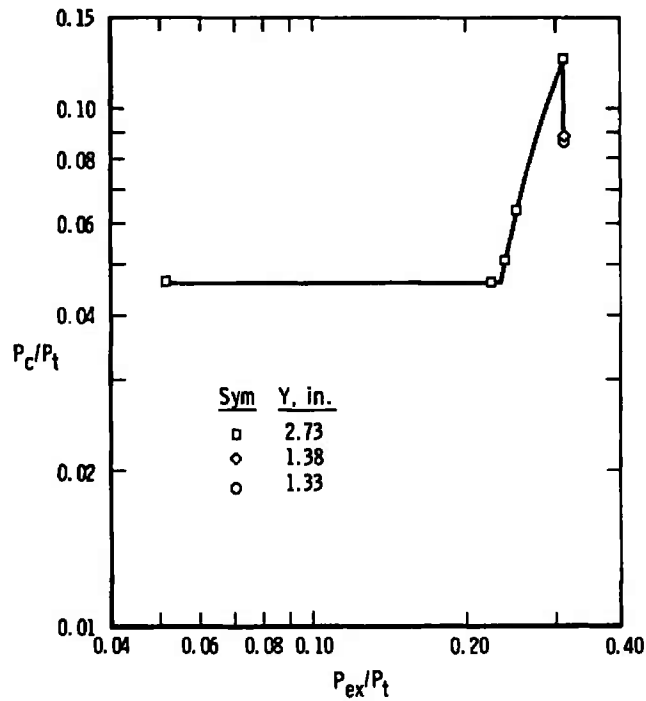


Figure 27. Single-angle centerbody configuration performance, $A_d/A^* = 5.756$, $m''/m' = 5$ percent.

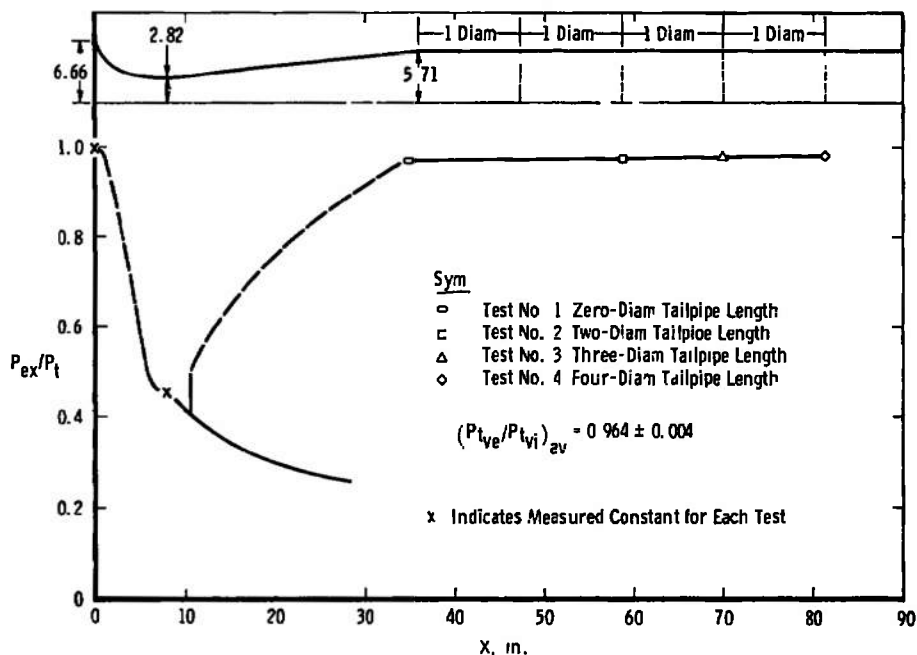
An important parameter in starting characteristics without secondary flow was the axial distance of the primary nozzle exit from the ejector second throat. Two limiting factors are believed to be the shocks generated by the centerbody in the supersonic stream and the impingement of the under-expanded jet on the duct wall. The shock reflections off the centerbody and the duct wall may limit the minimum value of test cell pressure attainable with a given configuration. Because the second-throat location changes with centerbody position, the intersection of the cylindrical and diverging ducts was used as the reference position for the second throat. This distance was not optimized in this study. The primary nozzle was moved to a position at which the minimum value of P_c was equal to that produced by the cylindrical diffuser and was maintained at that position for all configurations tested.

A variable second-throat configuration has been selected; however, the ejector inlet duct should be designed for maximum performance at

both military and augmented power operation. The authors are in agreement that a converging capture duct having a 6-deg to 10-deg total angle followed by a 6-in. length of 6-in.-diam duct and the single-angle centerbody will optimize the design. This inlet geometry would increase the secondary flow area along the mixing zone which would minimize mixing losses, thus producing smaller values of test cell pressure and correspondingly larger values of ejector static pressure rise ratios (P_{ex}/P_c) at all operating conditions. The existing ejector should be modified to incorporate the modified inlet duct and its performance verified experimentally.

4.9 THE EFFECT OF TAILPIPE ON VENTURI PRESSURE LOSS

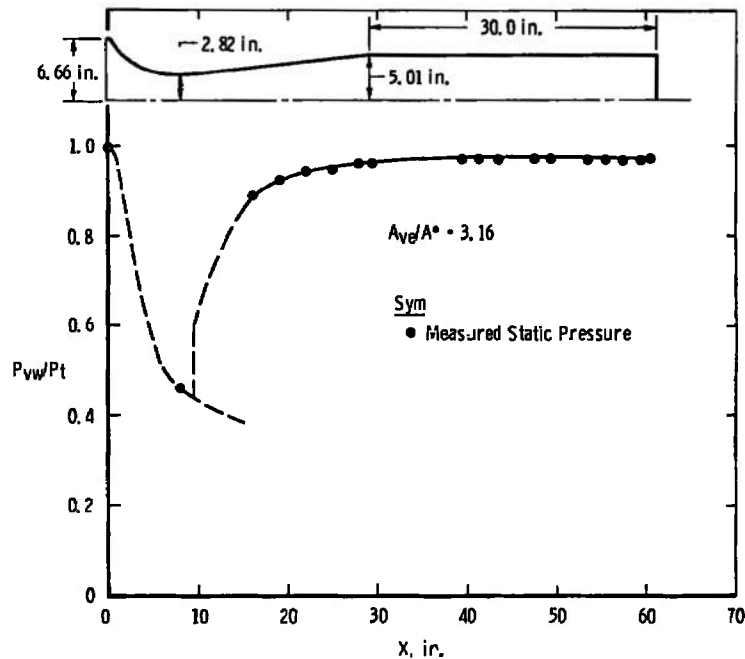
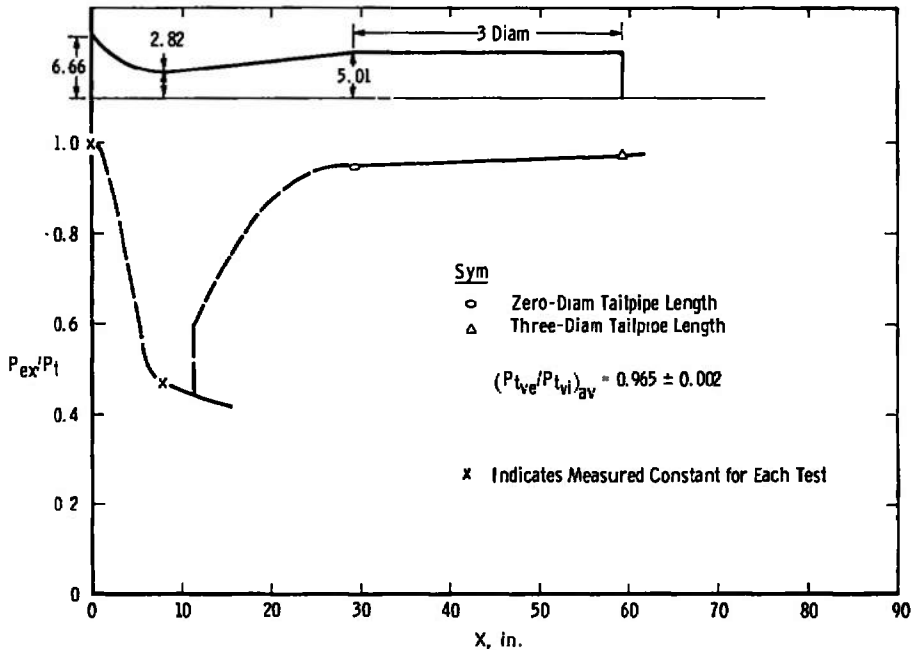
The results of the venturi tests are summarized in Fig. 28. The typical venturi without tailpipe is shown in Fig. 10 and with tailpipe in Fig. 15. A test was conducted for the venturi and for each length of tailpipe, either two, three, or four exit diameters. Figure 28 shows the effect of the tailpipe length on maximum pressure recovery while maintaining the critical-flow condition. Typical venturi static pressure survey, inlet, and exit total pressure profiles are presented in Figs. 29, 30, and 31, respectively. The tailpipe was shown to increase



a. $A_{ve}/A^* = 4.10$

Figure 28. Venturi performance.

the exit pressure ratio (P_{ex}/P_t) by only 2.9 and 0.8 percent for the area ratios A_{ve}/A^* of 3.16 and 4.10, respectively, which is an insignificant improvement over that of the venturi alone. Therefore, the addition of tailpipes to these venturis, operating with near ideal inlet flow conditions, is unjustified.



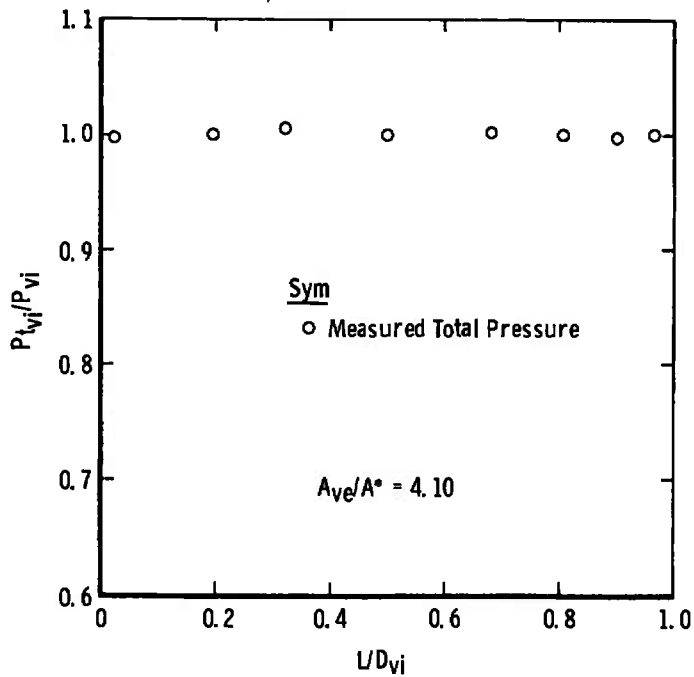


Figure 30. Typical venturi inlet total pressure profile.

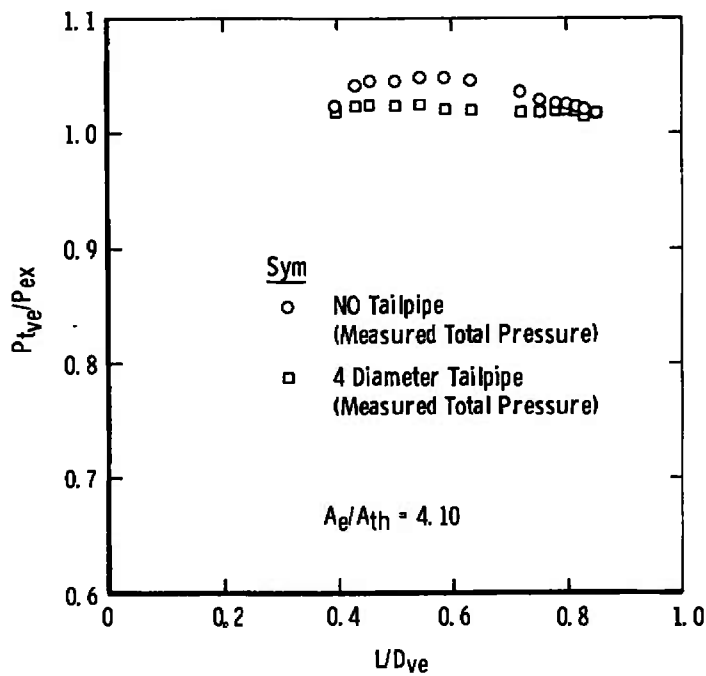


Figure 31. Typical venturi exit total pressure profile.

5.0 SUMMARY OF RESULTS

The results of the investigation to determine the performance of a centerbody-type variable-area second-throat ejector for application to a direct-connect turbojet test installation may be summarized as follows:

1. The static pressure rise ratio (P_{ex}/P_c) of the variable-area ejector exceeded by approximately 40 percent that of a constant-area ejector of equal length.
2. The optimum performance of the centerbody variable-area ejector was a function of the second-throat area.
3. The single-angle variable-area ejector could be adjusted for optimum performance at all operating conditions.
4. The shallow-angle diverging duct and blunt nose shallow angle centerbody arranged as a variable-area second-throat ejector produced the best results of all configurations tested.
5. The variable-area ejector was used to establish test cell pressure transients from standard sea-level static pressure (14.7 psia) to the minimum attainable by the installation while holding the ejector exit pressure (plant exhaust system pressure) at a value less than 1.0 psia.
6. Results of tests show that the addition of tailpipes to the venturis tested produced marginal performance improvements.
7. A truncated conical inlet duct configuration designed to improve cell pressure ratio during afterburner operation should be fabricated, and its predicted performance should be experimentally verified prior to the application of the variable-area ejector. Also the subsonic diffuser should be configured to fit within the available volume envelope of the test cells.

REFERENCES

1. Lewis, W.G.E. and Drabble, J. S. "Ejector Experiments." National Gas Turbine Establishment, Pyestock, Haunts. Report Number R-151, February 1954.
2. Uebelhack, H., Addy, A. L., Taylor, D., and Peters, C. E. "Supersonic Ejectors." Edited by Ginoux, J. J. AGARD-AG-163.

NOMENCLATURE

A	Area
C/B	Centerbody
D	Capture duct diameter
L	Ejector length
P	Pressure
X	Static pressure tap location
Y	Centerbody position
\dot{m}	Mass flow, lbm/sec

SUBSCRIPTS

c	Test cell
d	Duct
dw	Duct wall
ex	Exhaust
is	Isentropic
ne	Nozzle exit
ns	Normal shock
st	Second throat
t	Stagnation
ve	Venturi exit
vi	Venturi inlet
vm	Venturi throat
vw	Venturi wall

SUPERSCRIPTS

*	Nozzle throat
'	Primary flow
''	Secondary flow